Distribution Agreement

In presenting this thesis as a partial fulfillment of the requirements for a degree from Emory University, I hereby grant to Emory University and its agents the non-exclusive license to archive, make accessible, and display my thesis in whole or in part in all forms of media, now or hereafter know, including display on the World Wide Web. I understand that I may select some access restrictions as part of the online submission of this thesis. I retain all ownership rights to the copyright of the thesis. I also retain the right to use in future works (such as articles or books) all or part of this thesis.

Joshua P. Keller April 7, 2011

The Spread of Rabies in Raccoons: Numerical Simulations of a Spatial Diffusion Model

by

Joshua P. Keller

Alessandro Veneziani
Adviser

Department of Mathematics and Computer Science

Alessandro Veneziani

Adviser

James Nagy

Committee Member

Leslie Real

Committee Member

April 7, 2011

The Spread of Rabies in Raccoons: Numerical Simulations of a Spatial Diffusion Model

By

Joshua P. Keller

Alessandro Veneziani

Adviser

An abstract of
a thesis submitted to the Faculty of Emory College of Arts and Sciences
of Emory University in partial fulfillment
of the requirements of the degree of
Bachelor of Sciences with Honors

Department of Mathematics and Computer Science

2011

Abstract

The Spread of Rabies in Raccoons: Numerical Simulations of a Spatial Diffusion Model
By Joshua P. Keller

Raccoons, Procyon lotor, are a major carrier of the rabies virus in the Eastern United States. Compartmental models of disease provide an effective means for simulating epidemics of rabies and other diseases. However, most epidemiological models either do not consider individual movement at all or model it between discrete patches. Modeling movement as a continuous process provides several advantages, including the ability to incorporate spatially-oriented geographic and environmental factors affecting disease. We develop an SEIR model for disease spread with a diffusion component for continuous movement that is a system of partial differential equations (PDEs). We perform numerical simulations of the PDEs using the finite element method. We use the model to analyze a case study of the spread of rabies in raccoons in New York State since 1990.

The Spread of Rabies in Raccoons: Numerical Simulations of a Spatial Diffusion Model

By

Joshua P. Keller

Alessandro Veneziani

Adviser

A thesis submitted to the Faculty of Emory College of Arts and Sciences
of Emory University in partial fulfillment
of the requirements of the degree of
Bachelor of Sciences with Honors

Department of Mathematics and Computer Science

2011

Acknowledgements

I would like to thank Luca Gerardo-Giorda, who served as my co-advisor for this project and mentored me throughout the year and without whom this project would not have come to fruition. I would also like to thank my advisor, Alessandro Veneziani, for his support, guidance, and teaching throughout this project. I am grateful to the other members of my committee, James Nagy and Leslie Real, for their comments and suggestions on the work. I would like to thank Dr. Real for also providing the confirmed case data from New York State.

Contents

List of Figures

Chapter 1

Introduction

Rabies, a viral encephalomyelitis, is one of many infectious diseases that afflicts humans. Specific to mammals, the virus is the cause of thousands of deaths each year in some parts of India and Africa [32]. In the United States, human infections and fatalities are less common but the disease still persists in many non-human mammalian populations. Raccoons (*Procyon lotor*) are a major carrier of the disease across North America, though many foxes, bats, and skunks carry the disease as well [25, 32]. While a successful vaccine for humans and other mammals against rabies exists, and human fatalities are rare, the economic cost of widespread animal vaccination and the danger of rabies to threatened species makes understanding the spread of rabies in wildlife hosts important to epidemiologists [27, 32]. To study rabies and other infectious diseases, epidemiologists use mathematical models that simulate the transmission of disease throughout a population. These models allow for an understanding of the processes at work in an epidemic and are a means for prediction of future epidemics. The large majority of these epidemiological models have a compartmentalized design and are composed of a system of differential equations [2, 13].

These models, however, do not always account for the movement of animals from one region to another. But the daily movement and seasonal migration of animals can have

significant effects on the transmission of a disease. Though some aspects of infectious disease models are extremely well developed (e.g., rate of infection and stability of solutions for simple cases), describing the movement of individuals across a region in a mathematically rigorous and epidemiologically tractable way has been done in many different ways by different researchers [13, 10]. One canonical approach has been to discretize the population and geography into geopolitical units and consider the movement of individuals from unit to unit [13]. This approach, however, does not well represent the biological realities of animal movement, since animals do not move at the scale of geopolitical units. This study focuses on an alternative means for understanding individual movement as a continuous process across a continuous region. A mathematical model is formulated that combines a standard epidemiological model and a diffusion process to account for movement.

This results in a system of partial differential equations (PDEs) of parabolic form [10, 12, 22, 5]. As with many PDEs of practical interest, an analytical solution to this system cannot be explicitly computed. In fact, the domain of interest for our model is a complicated region of the plane, while analytical methods consider simple geometries such as rectangles and circles. For this reason, we resorted to a numerical approximation of the problem by reducing the differential equations to a (large) algebraic system. Standard numerical techniques for the algebraic problem allow us to compute the approximate solution.

Of the methods in common use, we employ the Finite Element (FE) method for the space variables and the Finite Difference (FD) method for the time dependence. FE method is in fact well-suited for complex geometries and features well known accuracy properties. The FD method, on the other hand, is a standard choice for time advancement (see e.g., [23]). These methods have been implemented in a code written by L. Gerardo Giorda in the MATLAB environment.

In order to investigate a practical application, we conducted a case study of rabies in the

state of New York. We produce a mathematical description of the region and approximate the solution to our mathematical model using FE. The numerical results are analyzed and compared to available data.

1.1 Outline

In **Chapter 2**, compartmental epidemiological models will be reviewed and developed from basic epidemiological principles. The biological and mathematical assumptions of each component of the model are highlighted. In **Chapter 3** we present the motivation for including spatial movement in these models and review past discrete models. Continuous-movement models are introduced, followed by the diffusion model of PDEs that is the focus of this study. In **Chapter 4** the Finite Element Method, which will be used to solve the model numerically, is described. The theoretical basis for this method is established and the method for computational implementation is given. A series of test cases will be presented, demonstrating the mathematical and epidemiological effects of each component in the model. In **Chapter 5** we analyze a case study of a rabies epidemic in New York state in the 1990s. A brief background of the disease epidemic is discussed and then the numerical implementation of the model is described. Results are interpreted with the aid of visualization software. Finally, we present conclusions about the effectiveness of the model and discuss future implications.

Chapter 2

Compartmental Models for Infectious Diseases

Compartmentalized models group a population into subpopulations, or 'compartments,' corresponding to the different status of each individual [19, 2, 13]. The standard groupings in epidemiology are: individuals that are not infected but who are susceptible to the disease (Susceptible, denoted by S), individuals infected with the disease but not yet able to infect others (Exposed, E), individuals infected with the disease and capable of infecting others (Infectious, I), and individuals who are neither susceptible nor infected (Recovered, R). The last category encompasses individuals who have acquired immunity by surviving the disease and those who have been vaccinated. Compartmentalized models originated from the early work of Hamer (1906), Ross (1908), and Kermack and McKendrick (1927), and have since been the focus of extensive study [13, 19, 8, 14, 1].

Different diseases have different epidemiological patterns of transmission and recovery. Four standard classes of epidemiological models are SIR, SIS, SEIR, and SEI. The acronym name of each model represents the general order of progression through the compartments

in that model, which is a function of the etiology of the disease.

$$\begin{aligned}
&\text{SIR (immunizing):} && \boxed{\text{Susceptible}} \longrightarrow \boxed{\text{Infectious}} \longrightarrow \boxed{\text{Recovered}} \\
&\text{SIS (non-immunizing):} && \boxed{\text{Susceptible}} \longrightarrow \boxed{\text{Infectious}} \longrightarrow \boxed{\text{Susceptible}} \\
&\text{SEI (latent, lethal):} && \boxed{\text{Susceptible}} \longrightarrow \boxed{\text{Exposed}} \longrightarrow \boxed{\text{Infectious}} \\
&\text{SEIR (latent, immunizing):} && \boxed{\text{Susceptible}} \longrightarrow \boxed{\text{Exposed}} \longrightarrow \boxed{\text{Infectious}} \longrightarrow \boxed{\text{Recovered}}
\end{aligned} \tag{2.1}$$

The population levels of each compartment are functions of time that change in value as individuals move between compartments and are denoted by $S(t)$, $E(t)$, $I(t)$, and $R(t)$.

Here we first consider the SIR model, establishing its components and then introducing the basic reproduction ratio. We then extend the results to the other standard models without vital dynamics. We conclude this chapter with a discussion and analysis of vital dynamics in compartmental models.

2.1 SIR

SIR models are used primarily for acute, immunizing diseases and serve as the basic form of epidemiological compartmental models [19].

The driving factor for the spread of disease, and thus for the movement between the groups in (2.1), is the infection of an individual. When an individual becomes infected, it is moved from the Susceptible class to the Infectious class. The guiding assumption of compartmentalized models is that the *per capita* rate of infection $\lambda(t)$ (also called the *force of infection* [13]) is proportional to the rate of contact between an infectious individual and a susceptible individual [8]. Thus, $\lambda(t)$ is proportional to both the rate of contact between

all individuals in a population, $\beta(t)$, and to the number of infectious individuals in that population, $I(t)$. The contact rate between individuals is typically assumed to be constant throughout time, and so we set $\beta(t) = \beta$. Thus the rate of newly infected individuals is given by the term $\lambda(t)S(t) = \beta S(t)I(t)$.

$$\boxed{\text{S(t)}} \xrightarrow{\beta S(t)I(t)} \boxed{\text{I(t)}}$$

Note that this formulation presumes that the population is homogeneously mixed and that each contact between a susceptible and an infectious individual is equally likely of causing infection. Though this assumption of infection as a density-dependent process has been criticized by Sterner *et al.*, it remains in widespread use [32].

Once infected, there is a period of time that an individual remains infectious until that individual recovers and becomes immune, an event that removes them from the Infectious class to the Recovered class. We define this recovery rate to be η, where η^{-1} is the average duration of infection. The number of individuals recovering from the disease in a unit of time is proportional to the current number of infected individuals, and so the term $\eta I(t)$ is added to the model.

$$\boxed{\text{S(t)}} \xrightarrow{\beta S(t)I(t)} \boxed{\text{I(t)}} \xrightarrow{\eta I(t)} \boxed{\text{R(t)}}$$

These two processes together define the basic SIR model, which is given by this system of ODEs:

$$\begin{cases} \frac{dS(t)}{dt} = -\beta S(t)I(t) & S(0) = S^0 > 0 \\ \frac{dI(t)}{dt} = \beta S(t)I(t) - \eta I(t) & I(0) = I^0 > 0 \\ \frac{dR(t)}{dt} = \eta I(t) & R(0) = R^0 \geq 0 \end{cases} \tag{2.2}$$

Though an analytic solution to (2.2) cannot be obtained explicitly, an analysis of the system can lead to helpful epidemiological insight even without a numerical approximation

[13]. An examination of the equation $dI/dt = \beta S(t)I(t) - \eta I(t)$ reveals that the Susceptible population level of $S(t) = \eta/\beta$ is a threshold for the system. When $S(t) < \eta/\beta$, $I'(t) < 0$ and so the number of Infectious individuals declines. If, on the other hand, $S(t) > \eta/\beta$, then $I'(t) > 0$ and an epidemic occurs. Because $S(t) \geq 0$ and $I(t) \geq 0$ for all t, the equation $dS/dt = -\beta S(t)I(t)$ implies that the Susceptible population is always non-increasing. Thus even if $S(t) > \eta/\beta$ and an epidemic occurs, the Susceptible population will eventually fall below the threshold η/β and the epidemic will die out.

The inverse of this threshold is related to a fundamental epidemiological parameter, the basic reproductive ratio R_0. Formally defined as the number of secondary infections generated by a single infectious individual in an entirely susceptible population, the value of R_0 for the system (2.2) is given by

$$R_0 = \frac{\beta N}{\eta}, \tag{2.3}$$

where N is the total population. Using this definition we can rewrite the threshold for the model with R_0. If the entire population is assumed to be initially susceptible, then an epidemic can only occur if $S^0 = N > \eta/\beta$. Substituting R_0 into this relation gives $R_0 > 1$. This result is intuitive, since if an infectious individual only infects less than one individual on average, then the disease should die out, while if they infect more than one individual, an epidemic should occur.

The formulation for R_0 given above in (2.3) is specific to compartmentalized models of the form (2.2). The exact value of R_0 for different diseases has been calculated using numerous algorithms for different models and actual epidemiological data, with the results often being quite different (we refer the reader to Heffernan *et al.* [9] for a more complete discussion). For that reason, R_0 is often better treated as a threshold for the propagation of a disease than the true number of secondary cases generated by an infectious individual.

Though these limitations on R_0 mean one must use caution when using it to compare

diseases and models, the formulation of R_0 given above provides useful insight to the mathematical models used here.

2.2 SIS, SEIR, SEI

The other three models are similar to the SIR, but modify or add epidemiological relations. The SIS models are used for diseases that do not provide immunity for those who survive the disease. Thus when an individual recovers from the infection, instead of moving to the Recovered compartment, they return to the Susceptible class. Since the process of recovery is similar to the SIR, only the destination compartment is different, the same term $\eta I(t)$ is used here.

$$\boxed{\text{S(t)}} \underset{\eta I(t)}{\overset{\beta S(t)I(t)}{\rightleftarrows}} \boxed{\text{I(t)}}$$

The SIS model can be represented by the following coupled differential equations:

$$\begin{cases} \frac{dS(t)}{dt} = \eta I(t) - \beta S(t)I(t) & S(0) = S^0 > 0 \\ \frac{dI(t)}{dt} = \beta S(t)I(t) - \eta I(t) & I(0) = I^0 > 0. \end{cases}$$

For many diseases, when an individual becomes infected they are not immediately capable of infecting others since the disease must incubate and propagate within the host. In such situations the SEIR model is used and a newly infected individual is placed in the Exposed category before being moved on to the Infectious compartment. The length of this latency period, σ^{-1}, determines the rate σ at which individuals become infectious. By multiplying this rate by the population of the Exposed compartment we obtain the term $\sigma E(t)$.

$$\boxed{\text{S(t)}} \xrightarrow{\beta S(t)I(t)} \boxed{\text{E(t)}} \xrightarrow{\sigma E(t)} \boxed{\text{I(t)}} \xrightarrow{\eta I(t)} \boxed{\text{R(t)}}$$

Interventions such as vaccination can alter the flow of individuals through these categories. Vaccination takes an individual from the Susceptible class and places them in the Recovered class (in this case sometimes called Removed, since the individual neither had the disease nor is capable of contracting it). If we let γ be the vaccination rate, we incorporate the term $\gamma S(t)$:

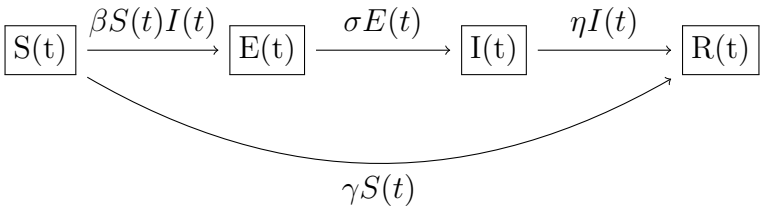

An SEIR model takes the form of the following equations, where $\gamma = 0$ if no vaccination is present.

$$\begin{cases} \frac{dS(t)}{dt} = -\beta S(t)I(t) - \gamma S(t) & S(0) = S^0 > 0 \\ \frac{dE(t)}{dt} = \beta S(t)I(t) - \sigma E(t) & E(0) = E^0 \geq 0 \\ \frac{dI(t)}{dt} = \sigma E(t) - \eta I(t) & I(0) = I^0 \geq 0 \\ \frac{dR(t)}{dt} = \eta I(t) + \gamma S(t) & R(0) = R^0 \geq 0 \end{cases}$$

However, in the case of rabies and several other diseases, an infected individual inevitably dies from the disease, and so there is no recovery term. Instead, we consider the fatality rate from infection ϕ, where ϕ^{-1} is the average time until death of an infectious individual. This gives the mortality term $\phi I(t)$ that removes individuals from the Infectious class.

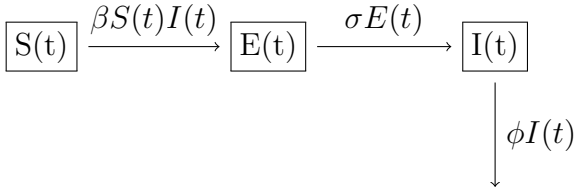

This SEI system can be represented by the following equations:

$$\begin{cases} \frac{dS(t)}{dt} = \beta S(t)I(t) & S(0) = S^0 > 0 \\ \frac{dE(t)}{dt} = \beta S(t)I(t) - \sigma E(t) & E(0) = E^0 \geq 0 \\ \frac{dI(t)}{dt} = \sigma E(t) - \phi I(t) & I(0) = I^0 \geq 0. \end{cases}$$

2.3 Vital Dynamics

The epidemiological factors considered above encompass acute infections that take place within a short enough time span that vital dynamics (birth and natural death) may be ignored. However for many diseases and epidemics, vital dynamics play a significant role and need to be included.

Inclusion of vital dynamics in a model usually incorporates a standard set of assumptions. New-born individuals are presumed to be susceptible to disease (transient passive immunity gained from the mother is ignored), and every member of the population is considered to be equally capable of contributing to the birth of new individuals. We consider natural death to be death by natural causes other than the disease of interest (e.g., predation, starvation). Because of this, the natural death rate is the same for individuals in all compartments. If infection with the disease has a known effect on the death rate of an individual, that effect is usually incorporated explicitly (as in the SEI model of the previous section). Thus if we let $N(t) = S(t) + E(t) + I(t) + R(t)$ and α denotes the birth rate and $\mu(t)$ the death rate at time t, we have the following relations:

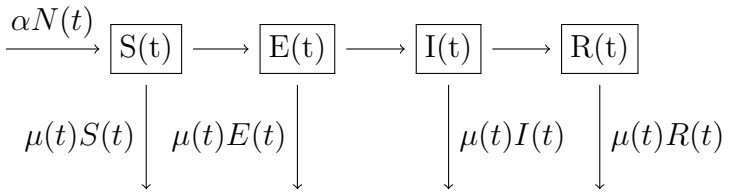

We can then write the system

$$\begin{cases} \frac{dS(t)}{dt} = \alpha N(t) - \beta S(t)I(t) - \mu(t)S(t) & S(0) = S^0 > 0 \\ \frac{dE(t)}{dt} = \beta S(t)I(t) - \sigma E(t) - \mu(t)E(t) & E(0) = E^0 \geq 0 \\ \frac{dI(t)}{dt} = \sigma E(t) - \eta I(t) - \mu(t)I(t) & I(0) = I^0 \geq 0 \\ \frac{dR(t)}{dt} = \eta I(t) - \mu(t)S(t) & R(0) = R^0 \geq 0. \end{cases} \tag{2.4}$$

2.3.1 Malthusian dynamics and stability

The most basic approach is to consider the case when the death rate is constant and equal to the birth rate, called neutural Malthusian dynamics. That is, when $\mu(t) = \alpha$. This means that $\alpha N(t) - \mu(t)S(t) - \mu(t)E(t) - \mu(t)I(t) - \mu(t)R(t) = 0$, and so the population size does not change. The inclusion of vital dynamics creates more complex dynamics and can enable the long-term persistence of disease (an endemic state) since the Susceptible class is being repopulated.

We now conduct a stability analysis for the system (2.4) with Malthusian dynamics. Since the population size is constant and $R(t)$ is not present in the first three equations of (2.4), we limit our analysis to the equations for the Susceptible, Exposed, and Infectious compartments and note that $R(t) = (S^0 + E^0 + I^0) - S(t) - E(t) - I(t)$. We begin by finding the equilibrium points, which are the solutions to this system (recall that $\mu = \alpha$):

$$\begin{cases} 0 = \mu N - \beta SI - \mu S \\ 0 = \beta SI - \sigma E - \mu E \\ 0 = \sigma E - \eta I - \mu I. \end{cases} \tag{2.5}$$

The third equation in (2.5) allows us to write E in terms of I:

$$E = \frac{\eta + \mu}{\sigma} I.$$

We then substitute this in the second equation and factor to obtain

$$0 = I\left(\beta S - (\eta + \mu) - \frac{\mu(\eta + \mu)}{\sigma}\right). \tag{2.6}$$

We note here that for the SEIR system (2.4) with vital dynamics [13],

$$R_0 = \frac{\sigma}{\sigma + \mu} \frac{\beta N}{\eta + \mu}.$$

Then the two possible possible solutions to equation (2.6) are

$$I_{e1} = 0 \quad \text{and} \quad S_{e2} = \frac{(\eta + \mu)(\sigma + \mu)}{\beta\sigma} = \frac{N}{R_0}.$$

Setting $I_{e1} = 0$ gives us the disease-free equilibrium $(S_{e1}, E_{e1}, I_{e1}, R_{e1}) = (N, 0, 0, 0)$. The presence of vital dynamics, however, means that there is also an endemic equilibrium, where the birth of new susceptibles allows the disease to continue to survive in the population. We solve for the endemic equilibrium by substituting $S_{e2} = N/R_0$ in the first equation of (2.5). This gives us

$$0 = N(\mu - \frac{\beta}{R_0} I - \frac{\mu}{R_0}).$$

Since we can ignore the trivial case $N = 0$, we have that

$$I_{e2} = \frac{\mu}{\beta}(R_0 - 1),$$

from which it follows

$$E_{e2} = \frac{\mu(\mu+\sigma)}{\beta\sigma}(R_0 - 1).$$

Since the population values must be non-negative, the endemic equilibrium can only exist if $R_0 > 1$. Li and Muldowney (1995) have shown that when $R_0 \leq 1$, the disease free equilibrium is stable, while when $R_0 > 1$ the endemic state is asymptotically stable [16]. We note that the equilibrium value of $S_{e2} = N/R_0$ means that we can expect the Susceptible population to be reduced by a factor of $(1 - 1/R_0)$ during an epidemic.

2.3.2 Non-Malthusian dynamics

For many animal populations, the number of individuals in a given area can affect the natural death rate due to such factors as competition. In such situations, the death rate is set up to be density-dependent, meaning the death rate $\mu(t)$ is proportional to the total number of individuals in the region, $N(t)$, at a given time. Rather than include a time-dependent function $\mu(t)$ in the differential equations, the convention is instead to separate the rate as $\mu(t) = \mu_0 N(t)$. By summing the equations in (2.4), we obtain the relation $dN/dt = \alpha N(t) - \mu(t)N(t)$. In the case of density-dependent mortality, $dN/dt = \alpha N(t) - \mu_0 N(t)^2$, which is a logistic equation with a stable equilibrium at the carrying capacity

$$L = \frac{\alpha}{\mu_0}. \tag{2.7}$$

This will result in the total population level being driven towards L, regardless of the initial population in each compartment.

In the case of rabies and several other diseases, an infected individual is not counted in as part of the reproducing population. Since the average survival time for an infected host is considerably shorter than the mean gestation period, no infected individuals is expected

to live long enough to give birth. If a pregnant individual does become infected late in gestation, the imminent death of the mother means survival is not likely for the newborn. In either case, we can safely remove infectious individuals from the reproducing population in the model and so define $N_r = S + E + R$ and have the Susceptible class grow by the term αN_r. When the disease infects only a small portion of the population this makes little difference, but for highly virulent diseases it can be a significant factor.

Making the birth and death rates temporally dependent can make the model more accurately reflect the seasonality of life cycles and available resources, but such complexities will not be considered here.

Chapter 3

Spatial Movement in SEIR Models

The models developed in the previous section all focused on single populations of individuals, aggregating all of the members into one of the four classes. These models provide information about the population-level statistics and the overall fate of the disease. However, they offer no information about the spread of the disease across regions, which is a critical factor in implementing intervention and prevention strategies. Instead, these single population models rely on the strong assumption that the entire population is homogeneously mixing. While reasonable in small areas, this does not well reflect reality across large geographic regions.

Many times, a separate model is applied to each of several connected geographic regions, giving a picture of the disease spread in what is called a *metapopulation model* [13]. Yet so long as a metapopulation model remains uncoupled, it provides little advantage over the single population model. This is because having distinct models for different geographic regions ignores the basic geographical and biological realities that connect the regions. Since animals (including humans) are mobile beings, the individuals in different regions may come into contact or interact with one another. Geographic features pass through regional boundaries, and environmental and meteorological forces can link even distant regions. A single infectious individual, if moved to a disease-free community, can start an epidemic, and so

incorporating the movement of hosts is key to a more accurate model. This necessitates some degree of coupling between regions, forming the *coupled* metapopulation model. Since such a model describes individual movement between discrete regions, we will refer to this as the *discrete approach*.

A second approach, and the focus of this study, is to consider the population to be a continuously-valued function across the entire domain, a strategy here termed the *continuous approach*. An introduction to both approaches is presented, highlighting the advantages and limitations of each, followed by a mathematical formulation for the continuous approach.

3.1 Discrete Approach

One of the most common approaches to incorporating spatial movement into an epidemiological model is to divide the domain into n discrete units, usually given by some geopolitical boundary (e.g., counties), that are then coupled to account for movement between them [17, 33, 20, 2]. For each location there is a different category S_i, E_i, I_i, R_i, for $i = 1, 2, ...n$, and thus a total of $4n$ coupled differential equations. The equations for different regions are coupled by a movement rate, such as ρ_{ij} that corresponds to the movement of individuals from location i to location j [29, 17, 30]. For example, in a discrete-movement analog to (2.4), the equations for the Susceptible category might read

$$\frac{dS_i}{dt} = \alpha(N_r)_i - \beta S_i I_i - \mu_i(t) S_i - \sum_{\substack{j=1 \\ j \neq i}}^{n} \rho_{ij} S_i + \sum_{\substack{j=1 \\ j \neq i}}^{n} \rho_{ji} S_j$$

This approach does have several advantages. While more complex than the single population case, the coupled system of ODEs reasonably incorporates the movements of individuals. Perhaps more importantly, most epidemiological data is aggregated across geopolitical regions, and so models discretized across space are convenient for fitting to such data. This

is especially true for diseases affecting humans, where local health agencies treat and report cases. This model is also appropriate when the population is known to be clustered, as in the distribution of humans in cities or livestock in farms. Another advantage of such models is that they can explicitly incorporate long-term transmission [29]. The movement coefficients described above are not limited to adjacent regions, but can incorporate "commuter" terms for distant regions. Again, this has advantages for models involving humans, where regular daily travel, sporadic long distance visits, and other non-random mixing can have a significant effect on disease spread [29]. Since however, animal hosts do not simply leap across large areas, this inclusion provides little advantage to many epidemiological models of non-human diseases. Many times stochastic processes are added to metapopulation models to account for unexpected and irregular movement patterns [13, 29].

Despite these advantages, there are several significant drawbacks to the discrete approach. Most basically, real-world individuals do not move on the scale of geopolitical units. While such units may be a convenient means for visualizing and documenting a disease, they are not representative of biological behavior. When individuals enter a region in the south, they are not immediately able to exit the region in the north, yet this model presumes that they are able to do so. Reducing the size of the regions (e.g., to census tract level or townships) can reduce this effect, but the fundamental assumption remains nonetheless. Also, all individuals within a single region are presumed once again to be homogeneously mixed and in contact with all of the individuals in the region. Thus a single infectious individual in a region is capable of infecting all susceptible individuals within that region, no matter how large the area may be and how sedentary that individual is. Furthermore, the population of each region must be of sufficient size for a deterministic model for that population to be appropriate [33]. With a discrete, sub-population approach, there is much greater possibility for localized extinction of a disease due to lower population levels. This

is balanced by the possibility of disease re-introduction, but significant care must be taken in determining the coupling parameters to create an appropriate balance between these two forces.

Spatially-discrete models can account for some physical barriers to movement, by factoring them into the movement rates ρ_{ij}. For example, the rate for two regions separated by a river could be reduced to account for the effect of that natural barrier. However, since the rates are only between the regions, only barriers that exist between the geopolitical boundaries may be included. Barriers to movement or transmission within a region are outside the consideration of these models.

While quite mathematically tractable and valuable when data already exists over a set of discrete regions, these discrete models have limitations that make them often less than ideal at modeling the spread of disease.

3.2 Diffusion: The continuous approach to movement

Rather than presume a set of discrete regions each with its own subpopulation, an alternative model is to consider a single population that varies continuously across space. The movement of individuals across this continuous domain can be modeled in multiple ways, and here we consider simple diffusion [10, 13, 26]. With a diffusion approach, the individuals are presumed to move in undirected manner across the entire region and to contact only those individuals in their immediate area, eliminating the need for the assumption of homogeneous mixing. This makes the continuous model well-suited to situations where the host population is known to be broadly dispersed.

Epidemiological models with a diffusion component have been analyzed theoretically [34, 6] and in applied contexts. Some of the early applied modeling was done by Noble (1974), who modeled the Black Death plague of the 1300s, and Murray et al. (1986), who

studied the spread of rabies in red foxes in Europe [22, 21]. More recently, Caraco *et al.* (2002) applied the diffusion approach to the spread of Lyme disease in the United States [3]. The study by Murray limited the random movement to the rabid individuals of the Infectious class, claiming that the territoriality of foxes would prevent the healthy members of the Susceptible class from wandering in a random manner. Here we propose expanding the diffusion to the movement of all individuals.

One advantage of the continuous approach to movement in the model is that it reflects the movement of individuals in reality; there are no spatial jumps. Individual movement is determined by the diffusion tensor, and so can be varied across the entire domain and for different categories of individuals.

The simplest case would be to allow movement equally in all directions, known as *isotropy*. This rate could be constant, or vary according to location in the domain. Thus, for example, the rate of movement can be reduced in mountainous regions or swamps. In addition to simply modifying the magnitude of the diffusion rate, a directional aspect can be incorporated, making the diffusion *anisotropic*. In the case of airborne individuals, factors such as global wind patterns can be introduced through a globally anisotropic condition that favors movement in a single direction. On the ground, the rate of movement across a river can be almost eliminated, while still allowing for movement tangential to the flow of the river. A simple way to include such anisotropy along a river is the use of the following function, which decreases the value of the diffusion coefficient ν from ν_H to ν_L rapidly as x approaches 0 (see Figure 3.1).

$$\nu_\epsilon(x) = \nu_H - (\nu_H - \nu_L)e^{1-\frac{\epsilon^2}{\epsilon^2 - x^2}} \tag{3.1}$$

If x is the distance to the river, this smoothly but quickly reduces the diffusion as the river is approached. The diffusion coefficients can also be adjusted for each class of individuals, allowing for rabid individuals to have a higher degree of movement, in accordance with the

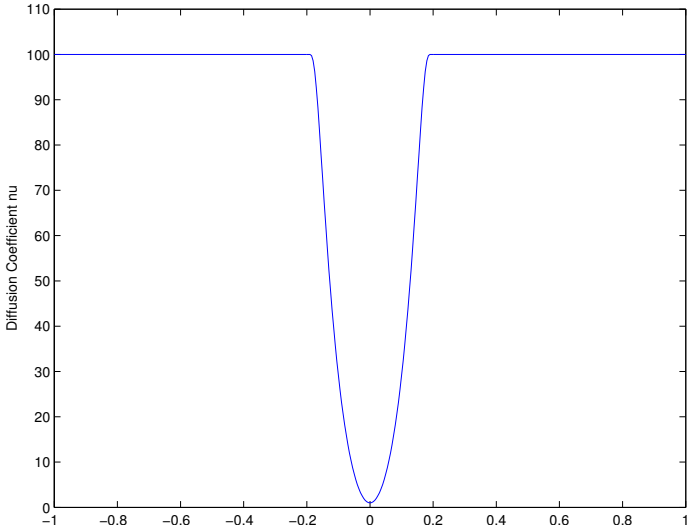

Figure 3.1: The graph of ν_ϵ from (3.1). Here $\nu_H = 100$, $\nu_L = 1$, and $\epsilon = 0.2$.

assumptions of Murray et al.

The mathematical formulation of diffusion is given by the addition of the Laplacian operator to the differential equations. The Laplacian is the divergence of the gradient of a function u, denoted by $\nabla \cdot \nabla u$, and corresponds to the sum of the unmixed second partial derivatives of that function. The addition of the Laplacian changes the traditional ordinary differential equation systems into systems of parabolic PDEs. These PDEs are in fact simple variants of the heat equation known as diffusion-reaction equations, for which many rigorous numerical methods exist [2, 23]. To solve accurately, however, the reaction-diffusion require more advanced mathematical theory, which will be covered in the next section, and that is perhaps part of the reason why they appear to be in less use than the discrete models [10].

By using a continuous space approach, there are no artificial effects of non-natural (e.g. sociopolitical) boundaries, while allowing for an extremely wide degree of freedom in incorporating spatially-dependent factors affecting disease spread. The epidemiological parameters discussed above can also be varied in a continuous manner across the domain, allowing for a richer degree of parameterization and fine-tuning. One critique of diffusion models has

been that they do not incorporate local behavior well [25]. But given sufficient information, heterogeneous variation in the geography and behavior can be incorporated at a fine scale.

3.3 The Mathematical model

By incorporating a diffusion process to account for individual movement, we arrive at the complete diffusion-driven SEIR epidemiological model that is the focus of this investigation. Rabies in raccoons can be represented by an SEIR model with fatal infections, density-dependent mortality, vaccination, and non-reproducing infectious individuals, diagrammed below.

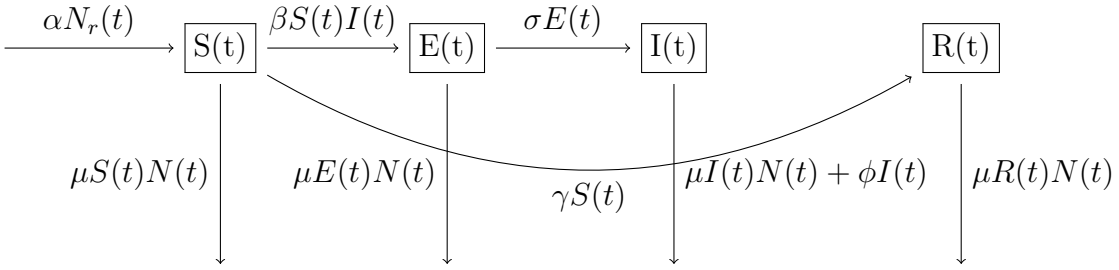

Translating these relations into differential equations and adding the diffusion term gives us the system of PDEs that will be the focus of this investigation. Since we are considering movement across a two-dimensional geographical domain, we let $\mathbf{x} = (x, y)$ represent the spatial location in the spatial domain Ω.

$$\begin{cases} \frac{\partial S(\mathbf{x},t)}{\partial t} = \alpha N_r(\mathbf{x},t) - \beta S(\mathbf{x},t)I(\mathbf{x},t) - \gamma S(\mathbf{x},t) - \mu S(\mathbf{x},t)N(\mathbf{x},t) + \nabla\left(\nu_S(\mathbf{x})\nabla S(\mathbf{x},t)\right) \\ \frac{\partial E(\mathbf{x},t)}{\partial t} = \beta S(\mathbf{x},t)I(\mathbf{x},t) - \sigma E(\mathbf{x},t) - \mu E(\mathbf{x},t)N(\mathbf{x},t) + \nabla\left(\nu_E(\mathbf{x})\nabla E(\mathbf{x},t)\right) \\ \frac{\partial I(\mathbf{x},t)}{\partial t} = \sigma E(\mathbf{x},t) - \phi I(\mathbf{x},t) - \mu I(\mathbf{x},t)N(\mathbf{x},t) + \nabla\left(\nu_I(\mathbf{x})\nabla I(\mathbf{x},t)\right) \\ \frac{\partial R(\mathbf{x},t)}{\partial t} = \gamma S(\mathbf{x},t) - \mu R(\mathbf{x},t)N(\mathbf{x},t) + \nabla\left(\nu_R(\mathbf{x})\nabla R(\mathbf{x},t)\right) \qquad \forall(\mathbf{x},t) \in \Omega \times (0,T) \end{cases} \tag{3.2}$$

$$N_r(\mathbf{x},t) = S(\mathbf{x},t) + E(\mathbf{x},t) + R(\mathbf{x},t)$$

$$N(\mathbf{x},t) = S(\mathbf{x},t) + E(\mathbf{x},t) + I(\mathbf{x},t) + R(\mathbf{x},t)$$

$$\frac{\partial}{\partial n}S(\mathbf{x},t) = \frac{\partial}{\partial n}E(\mathbf{x},t) = \frac{\partial}{\partial n}I(\mathbf{x},t) = \frac{\partial}{\partial n}R(\mathbf{x},t) = 0 \qquad \forall(\mathbf{x},t) \in \partial\Omega \times (0,T)$$

$$S(\mathbf{x},0) = S^0 \geq 0, \quad E(\mathbf{x},0) = E^0 \geq 0, \quad I(\mathbf{x},0) = I^0 \geq 0, \quad R(\mathbf{x},0) = R^0 \geq 0 \qquad \forall \mathbf{x} \in \Omega$$

Since we consider diffusion in space, but not in time, the Laplacian operators above operate only on the spatial variable $\mathbf{x}$ and not on the time variable t. Since the spatial variable is 2-dimensional, the diffusion tensor $\nu(\mathbf{x})$ can be represented by a 2×2 matrix.

The spatial boundary conditions given above are homogenous Neumann conditions, which means that there is no movement normal to the boundary of the region. The Neumann conditions, which make the domain an isolated region, were chosen to prevent the population from simply escaping from the region through diffusion. While the geographic regions investigated are not completely isolated, the Neumann conditions allows us to assume a perfect balance of migration and emigration $N_{in} = N_{out}$ for the region. We assume that adjacent regions are undergoing similar dynamics, and so this migration balance holds for each epidemiological

category.

A value of R_0 can be found for (3.2) in a similar way that it was found for the SIR system (2.2). Here the exposed class and the demographic terms lower the value from the simple case, and we have the formula [7]:

$$R_0 = \frac{\sigma}{\sigma + \mu L} \frac{\beta L}{\phi + \mu L} = \frac{\sigma}{\sigma + \alpha} \frac{\beta L}{\phi + \alpha}, \tag{3.3}$$

where $L = \alpha/\mu$ is the carrying capacity. Again, this value is best used as a threshold indicator rather than an exact predictor of secondary infections. The above formulation also excludes the diffusion component for ease of computation. When incorporating spatial heterogeneity, the true value of R_0 is usually slightly higher than this calculated value [19].

Chapter 4

The Numerical Method

There are many approaches for solving partial differential equations, but in general it is difficult or impossible to find an explicit representation for a solution. Instead, numerical methods provide approximate solutions to boundary value problems and initial and boundary value problems. Here we mention two approaches for solving PDEs numerically: *Finite Difference* (FD) and *Finite Element* (FE) methods. Both approaches transform the PDEs into algebraic equations that can be solved using computational methods from numerical linear algebra, however they do so in different ways. While they do not provide analytic solutions, the approximations these methods provide make them useful for engineering and physical applications [11, 18]. Though they can be quite accurate, both methods incur error from the numerical method (discretization errors) and from the actual computation of the results (rounding errors).

The finite difference method assumes the solution of the PDE holds across the domain (the strong formulation) and approximates the derivatives directly at a series of grid points using differences between discrete values. For linear and rectangular domains, this approach is well-developed and powerful, but it is less suited for irregular domains and higher dimensions. Finite differences also requires assumptions of regularity on the functions and derivatives

involved. Here we use FD for solving the time-component of (3.2), but do not use it for the spatial spread.

The Finite Element method instead approximates the function over a series of elements, usually two-dimensional polygons or three-dimensional polyhedrons. FE is based upon the weak formulation of the PDE, which assumes a solution holds in the domain when weighted by a test function. There are several advantages to using FE, two of which are important here [15]: (i) the FE method is easily adaptable to irregular domains and (ii) the accuracy of the method is mathematically completely assessed.

The computation of a solution to a partial differential equation using FE generally follows these steps. First, in *preprocessing*, the domain must be discretized into a suitable mesh. Next, in the *assembly* stage, the matrix corresponding to the discretization of the problem is computed. This is followed by a *time-advancement* step, which includes the solving of an algebraic system at each time step. Lastly, the computed data is made concise and presentable in *post-processing*, which usually involves the creation of images.

For the approximation of (3.2), the finite element method was used in space, and finite difference method in time. The computations were done within MATLAB, using a code developed by L. Gerardo Giorda. We present the requisite theory behind the finite element formulation of the problem and its implementation in MATLAB. First in Section 4.1 we consider the spatial discretization of the domain and the preprocessing step of mesh generation. In Section 4.2 we present the weak formulation of the problem, followed by the algorithm for matrix assembly in Section 4.3. In Section 4.4 we present the time-advancement scheme, and lastly the postprocessing step of data visualization in Section 4.5.

4.1 Space discretization

We must first divide the domain Ω (assumed to be a closed, bounded connected set) into a suitable finite collection of two-dimensional polygons. While in principle different shapes of elements are possible, here we consider one of the most versatile, triangulation. We consider the triangulation T of Ω given by

$$\Omega = \bigcup_{K \in T} K$$

where each $K \subseteq \mathbb{R}^2$ is a triangular finite element. The triangles K must each follow a simple set of conditions (conformal FE):

(i) no triangle may overlap with another

(ii) no node may be in the interior of another triangle

(iii) no node may exist on the edge of another triangle.

In general, it is possible to consider curvilinear triangles, which are particularly useful for complicated geometries (e.g., curved surfaces). Here, we use simple rectilinear triangles identified by the position of the 3 vertices. In particular, we consider triangles in the plane of a reference element $\hat{K}$ with vertices $(0,0)$, $(1,0)$, and $(0,1)$ and edges given by the equations

$$\begin{cases} \hat{\phi}_1 & = 1 - \hat{x} - \hat{y} \\ \hat{\phi}_2 & = \hat{x} \\ \hat{\phi}_3 & = \hat{y}. \end{cases} \tag{4.1}$$

We can then regard each generic triangle K as the result of an affine transformation of $\hat{K}$ according to the function $T_K(\hat{K}) = \begin{cases} x_K = x_K(\hat{x}, \hat{y}) \\ y_K = y_K(\hat{x}, \hat{y}) \end{cases}$. This allows for computations to be performed on the reference element and then transformed to K according to T_K (see Figure

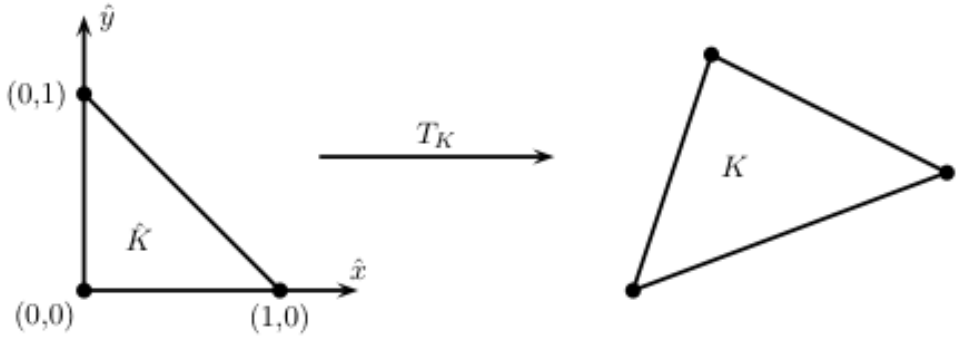

Figure 4.1: The reference triangle $\hat{K}$ and the map T_K.

4.1.

4.1.1 Mesh generation

There are many ways in practice to generate a mesh of a domain. Since these computations are performed in MATLAB, one of the simplest is to define a grid of points across the domain and use the `delaunay` function, which generates a Delaunay triangulation on the domain. Delaunay triangulations are triangulations such that no node is in the circumcircle of any element, a condition with maximizes the smallest angle in each triangle. Note that the grid of points need not be regular to generate such a mesh.

For non-rectangular domains, which can be difficult to define in MATLAB, there are many software packages that can create triangular meshes. One such program is Netgen[1]. Netgen includes geometries for standard geometrical shapes and supports importing CAD designs, but can also create custom geometries through interpolation. This last feature was used in this study to generate the irregular domains for the case study in the state of New York. By interpolating a series of points along the domain boundary with linear functions, NetGen defines a custom geometry that can then be meshed. One further advantage of NetGen and

[1]http://sourceforge.net/projects/netgen-mesher/

similar programs is the degree of control available for the size and shape of the mesh.

4.2 Weak Formulation of the Problem

In finding an approximate solution to (3.2), we consider the single function u to represent the values of all four compartments. Letting $u = u(x, y, t)$, this allows us to rewrite (3.2) as

$$\frac{\partial u}{\partial t} - \nabla \cdot (\nu(x, y)\nabla u) = f(u).$$

In this formulation, $f(u)$ represents the epidemiological factors and relations found in (3.2). We then weight the equation using a test function $v \in V$ for some functional space V and integrate over the domain, giving

$$\int_\Omega \frac{\partial u}{\partial t} v - \int_\Omega \nabla \cdot (\nu \nabla u) v = \int_\Omega f v. \tag{4.2}$$

The Gauss divergence Theorem states that

$$-\int_\Omega \nabla \cdot (\nu \nabla u) v = -\int_\Gamma \nu(\nabla u \cdot \mathbf{n}) v + \int_\Omega \nu \nabla u \cdot \nabla v,$$

where $\mathbf{n}$ represents the vector normal to the domain boundary. Thus (4.2) above can be rewritten as

$$\int_\Omega \frac{\partial u}{\partial t} v - \int_\Gamma \nu(\nabla u \cdot \mathbf{n}) v + \int_\Omega (\nu \nabla u) \nabla v = \int_\Omega f v$$

Because (3.2) has homogenous Neumann boundary conditions, $\nabla u \cdot \mathbf{n} = \frac{\partial u}{\partial \mathbf{n}} = 0$, and so the integral over the boundary Γ vanishes. We are then left with the problem to find $u \in V$, such that

$$\int_\Omega \frac{\partial u}{\partial t} v + \int_\Omega (\nu \nabla u) \nabla v = \int_\Omega f v \quad \forall v \in V. \tag{4.3}$$

This gives us the weak formulation of the mathematical model (3.2). A well-posedness analysis of equation (4.3) can be found in Salsa (2009) [28]. To perform the approximation of the problem, we decide to select v in a subspace V_h of V which can be easily handled for the numerical solution. In particular, we select piecewise linear functions, i.e.

$$V_h := \{v_h \in L^2(\Omega) | v_{h|K} \in \mathbb{P}^1, \forall K \in T_K\}.$$

By making V_h the space of square-integrable linear polynomials over our domain, we are then guaranteed a solution to the problem of finding $u_h \in V_h$ such that

$$\int_\Omega \frac{\partial u_h}{\partial t} v_h + \int_\Omega (\nu \nabla u_h) \nabla v_h = \int_\Omega f v_h \quad \forall v_h \in V_h.$$

Since we have discretized the domain into finite elements defined globally by N nodes, we can write u_h in terms of basis functions over these nodes: $u_h(x, y, t) = \sum_{j=1}^{N} u_j(t)\phi_j(x, y)$ and select $v_h(x, y) = \phi_i(x, y)$ for $i = 1, 2, ...N$. Note that here we assume that time and space are independent, since the domain of interest is fixed in time.

By substituting in the selection of v_h, we have

$$\int_\Omega \frac{\partial u_h}{\partial t} \phi_i + \int_\Omega (\nu \nabla u_h) \nabla \phi_i = \int_\Omega f \phi_i \quad \text{for } i = 1, 2, ...N.$$

Then substituting for u_h we obtain

$$\int_\Omega \frac{\partial}{\partial t} \sum_{j=1}^{N} u_j(t)\phi_j\phi_i + \int_\Omega \left(\nu \nabla \sum_{j=1}^{N} u_j(t)\phi_j \right) \nabla \phi_i = \int_\Omega f \phi_i \quad \text{for } i = 1, 2, 3, ..N. \tag{4.4}$$

In general, there are many possible ways to approximate the integral on the right hand side

of this equation using quadrature rules of the form

$$\int_\Omega f\phi_i = \int_\Omega f(u(x_q, y_q))\phi(x_q, y_q)w_q$$

where w_q are weights and the subscript q indexes the quadrature nodes. Here we use a linear interpolation of the function $f = \sum_{j=1}^{N} f_j\phi_j$, where $f_j = f(u_j(t))$. Substituting this approximation in (4.4) gives us

$$\sum_{j=1}^{N}\left(\frac{du_j(t)}{dt}\int_\Omega \phi_j\phi_i + u_j(t)\int_\Omega(\nu\nabla\phi_j)\nabla\phi_i\right) = \sum_{j=1}^{N} f(u_j(t))\int_\Omega \phi_j\phi_i \quad \text{for } i = 1, 2, 3, ..N. \tag{4.5}$$

Now (4.5) may be converted to a linear system by writing u as a vector whose entries are the values of u in the nodes, i.e. $\mathbf{u}_i = u(x_i)$. We call $M = \int_\Omega \phi_j\phi_i$ the *mass matrix* and $A = \int_\Omega(\nu\nabla\phi_j)\nabla\phi_i$ the *stiffness matrix*. The method for evaluating the entries of these matrices will be covered in the following section. With the above substitutions, we have the linear ordinary differential equations

$$M\frac{d\mathbf{u}}{dt} + A\mathbf{u} = M\mathbf{f}, \tag{4.6}$$

which can be solved with the standard numerical techniques described in the Section 4.4.

4.3 Assembly of Stiffness and mass matrix

To assemble the stiffness and mass matrices M and A, we evaluate the integrals element-wise, noting that

$$\int_\Omega(\nu\nabla\phi_j)\nabla\phi_i = \sum_{K\in T}\int_K(\nu\nabla\phi_j)\nabla\phi_i \quad \text{for } i, j = 1, 2, ...N.$$

For each element K, we write $\nabla\phi_i$ as a 2×3 matrix $\boldsymbol{\phi}^K$, where each column represents the gradient of the basis function centered in one node of the element. Thus we have

$$\int_K (\nu\nabla\phi_i)\nabla\phi_j = \int_K (\nabla\boldsymbol{\phi}^K)^T(\nu\nabla\boldsymbol{\phi}^K). \tag{4.7}$$

Since each element K is affine-transform of the reference element $\hat{K}$, we can further reduce the integral (4.7) to the reference basis of $\hat{K}$. If $p_K^1 = (x_1, y_1)$, $p_K^2 = (x_2, y_2)$, and $p_K^3 = (x_3, y_3)$ are the three vertices of K, then $J_K = \begin{bmatrix} x_2 - x_1 & x_3 - x_1 \\ y_2 - y_1 & y_3 - y_1 \end{bmatrix}$ is the Jacobian matrix of T_K. Now we write $\nabla\boldsymbol{\phi}^K = J_K^{-T}\nabla\hat{\boldsymbol{\phi}}$. Since the $\hat{\boldsymbol{\phi}}$ are given by (4.1), we have that $\nabla\hat{\boldsymbol{\phi}} = \begin{bmatrix} -1 & 1 & 0 \\ -1 & 0 & 1 \end{bmatrix}$. This allows us to write (4.7) as

$$\int_K (\nabla\boldsymbol{\phi}^K)^T(\nu\nabla\boldsymbol{\phi}^K)d\mathbf{x} = \int_{\hat{K}} (J_K^{-T}\nabla\hat{\boldsymbol{\phi}})^T\nu J_K^{-T}\nabla\hat{\boldsymbol{\phi}}J_K d\hat{\mathbf{x}} \tag{4.8}$$

We then use Gaussian quadrature to approximate all of the integrals. By letting $|K|$ be the area of element K, $\{p_K^{ij}, i, j = 1, 2, 3\}$ be the midpoints joining p_K^i and p_K^j, and p_K^{123} be the centroid of K, we have the following quadrature.

$$\int_K g(\mathbf{x}) \approx \frac{|K|}{60}\left(3\sum_{i=1}^{3} g(p_K^i) + 8\sum_{1\le i<j\le 3} g(p_K^{ij}) + 27g(p_K^{123})\right)$$

Using this quadrature for the integral in (4.8), we can now compute the 3×3 stiffness matrix for the element K:

$$\int_K (\nabla\boldsymbol{\phi}^K)^T(\nu\nabla\boldsymbol{\phi}^K) =: A_K$$

We then assemble the global stiffness matrix A by

$$a_{ij} = \sum_{K \in T'_K} (A_K)_{rs}$$

where T'_K is the set of all $K \in T_K$ such that the ith and jth nodes in T_K are the rth and sth vertices of K.

To assemble the Mass matrix $M = \int_\Omega \phi_j \phi_i$ we again proceed element-wise. It can be shown that

$$\int_K \phi_r \phi_s = \begin{cases} \frac{|K|}{6} & \text{if } r = s \\ \frac{|K|}{12} & \text{if } r \neq s \end{cases} \qquad \text{for } r, s = 1, 2, 3.$$

Thus the mass matrix for each element K is given by $M_K = \frac{|K|}{12} \begin{bmatrix} 2 & 1 & 1 \\ 1 & 2 & 1 \\ 1 & 1 & 2 \end{bmatrix}$ and the entries of the preliminary global mass matrix are given by

$$m'_{ij} = \sum_{K \in T'_K} (M_K)_{rs}.$$

In order to gain numerical stability from a diagonally dominant matrix, we lump each row of the preliminary mass matrix onto the diagonal, forming the (final) global mass matrix, whose entries are given by (see e.g., [24]):

$$m_{ij} = \begin{cases} \sum_{k=1}^{N} m'_{ik} & \text{if } i = j \\ 0 & \text{otherwise.} \end{cases}$$

4.4 Time Advancement

After the stiffness and mass matrices have been created, the next step in the algorithm is the time-advancing portion. We proceed in time using an implicit-explicit (IMEX) scheme, where we advance implicitly with respect to spatial diffusion and explicitly with respect to time using finite differences. Splitting diffusion-reaction systems in this manner is a well-developed computational technique, especially when the time-dependent portion of the system is non-linear, as is the case here (see e.g., [11, 18]).

Time is discretized in a simple linear manner, splitting the interval $(0, T)$ into increments of size Δt. From (4.6) we have that $Md\mathbf{u} = M\mathbf{f}\Delta t - A\mathbf{u}\Delta t$. Since we are proceeding implicitly with respect to diffusion and explicitly with respect to time, at the nth time step we must solve

$$M\mathbf{u}^n = M\mathbf{u}^{n-1} + M\mathbf{f}^{n-1}\Delta t - A\mathbf{u}^n\Delta t.$$

We obtain the next value of $\mathbf{u}^n$ by solving the linear system

$$(M + A\Delta t)\mathbf{u}^n = M\mathbf{u}^{n-1} + M\mathbf{f}^{n-1}\Delta t.$$

In MATLAB this algorithm is implemented in the following manner:

$H = A * \Delta t + M$

for $n = 1 : \Delta t : T$

$\mathbf{f}_{n-1} = \mathbf{f}(\mathbf{u}_{n-1})$ %Linearization of the nonlinear term

$\mathbf{g}_n = \Delta t * M * \mathbf{f}_{n-1} + M * \mathbf{u}_{n-1}$

$\mathbf{u}_n = H \backslash \mathbf{g}_n$ %Solution of the linear system

end

4.5 Data Visualization

The last step in this process requires the post-processing of the data with visualization software. MATLAB includes basic visualization capabilities, which are used here for the test cases of the next section and for a portion of the New York case study. The visualization program Paraview[2] provides greater flexibility in visualization and is used to display the simulation results of the case study.

4.6 Unit Square Simulations: The Effect of Parameter Variation

In order to demonstrate the effect of different parameter values on disease dynamics, we conduct a series of test-case simulations of (3.2) on the unit square. For these simulations, we divide the unit square into a 51×51 grid of nodes and form a triangular mesh of 5000 elements using MATLAB's `delaunay` function. Also for these simulations, we consider the spread of disease in the absence of vaccination (that is, $\gamma = 0$), which allows us to consider only the Susceptible, Exposed, and Infectious classes. Furthermore, we presume that the diffusion coefficient is the same across compartments. That is, we set $\nu_S = \nu_E = \nu_I =: \nu$. While in principle any of the parameters in (3.2) may be varied, several correspond to biological and epidemiological properties that can be estimated from observation or experimentation (e.g., average life span, incubation period of a disease) and thus have limited variability. Two parameters in the model that are subject to frequent variation are the diffusion coefficient ν and the contact rate β (and therefore the force of infection). In this section, we first investigate the epidemiological model with general isotropic diffusion and then present a systematic comparison between the effects of altering ν and β. We conclude these test-case

[2] http://www.paraview.org/

simulations by presenting simulations with spatially-varying and anisotropic diffusion.

Before varying the parameters, we investigate a numerical approximation of (3.2) with simple isotropic diffusion to highlight the implications of the assumptions in the model. For this simulation we set $\alpha = 0.2$, $\beta = 0.04$, $\sigma = 0.33$, $\phi = 0.0714$, $\mu = 0.002$, and $\nu = 10^{-3}$. From (2.7) and (3.3) we know that the carrying capacity of this model is $L = 100$ and the basic reproductive ratio is $R_0 \approx 9.18$. For the simulation, we consider the initial population to be entirely susceptible ($S^0 = 100$, $E^0 = I^0$), except for a small circular "source region" centered at $(0.2, 0.5)$ with radius 0.05. Within this source region, $S^0 = 90$, $E^0 = 9$, and $I^0 = 1$. The population level for each compartment at two points in time are presented in Figure 4.2.

The images in this figure show the propagation of the disease across the domain in a wave-like manner. The shape of this wave reflects the isotropic nature of the diffusion: movement is equal in all directions. The peak of the front at any arbitrary location occurs first in the Exposed category, followed shortly thereafter by the peak in Infectious individuals (see Figure 4.3). This follows the assumptions of (3.2) since infected individuals move first to the Exposed class before moving to the Infectious compartment. Also as expected, the peak of the number of Exposed individuals exceeds the peak number of Infectious individuals. This can be attributed to the natural death term from the Exposed class, which means that unless the latency period is infinitesimal, there will be individuals who die before ever reaching the Infectious class.

In this particular simulation, the force of infection is so high that the Susceptible class is entirely eliminated by the advancing disease front. There is a birth term present, and though small in magnitude, one might expect it to allow the Susceptible class to be repopulated and an endemic state reached. But recall that the birth term in (3.2) is αN_r, which means Infectious individuals cannot contribute to the birth of new individuals, and so the virulence

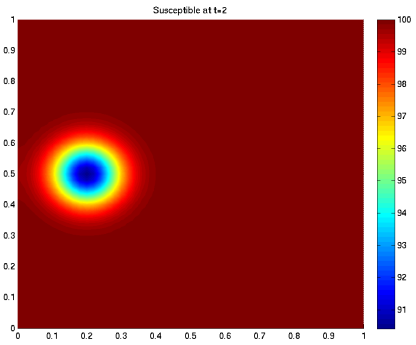

(a) Susceptibles at t=2

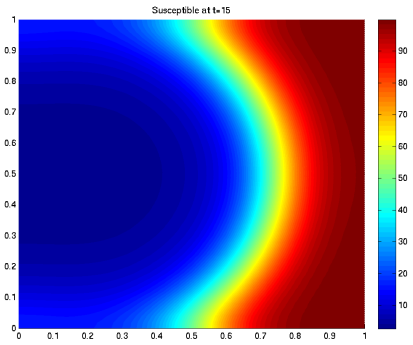

(b) Susceptibles at t=15

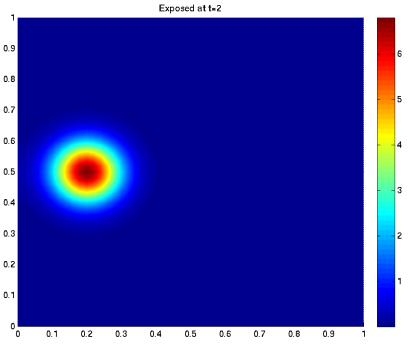

(c) Exposed at t=2

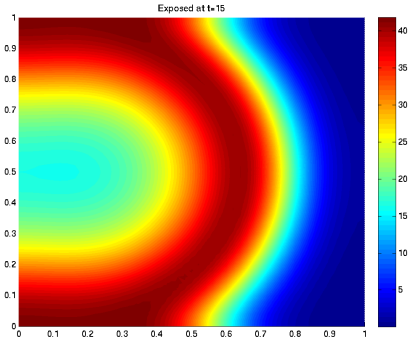

(d) Exposed at t=15

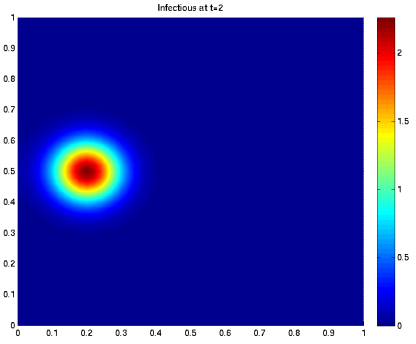

(e) Infectious at t=2

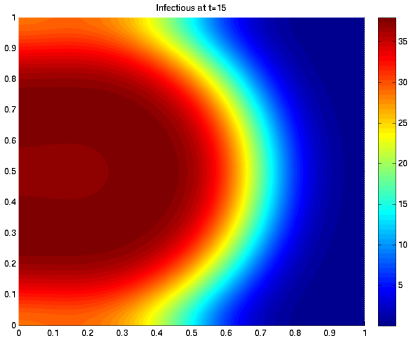

(f) Infectious at t=15

Figure 4.2: Population levels at two time steps for a simulation of (3.2) on the unit square.

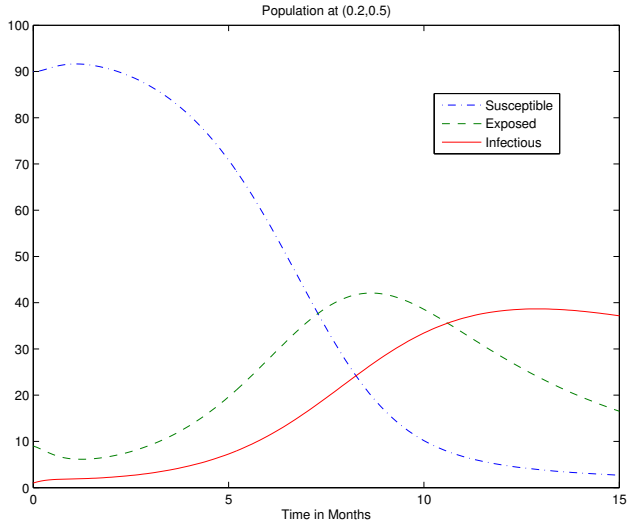

Figure 4.3: Population at the point (0.2,0.5)

of the disease causes the entire population to move towards extinction.

In Figures 4.4 and 4.5 we present a systematic variation of the contact rate β and diffusion coefficient ν to demonstrate the relative effect of altering each. For this sensitivity comparision, $\beta = \{0.001, 0.005, 0.01, 0.05\}$ and $\nu = \{0.00005, 0.00001, 0.0005, 0.001\}$, with the other parameters remaining the same as in the first example. Each figure represents the population of Susceptibles at $t = 15$, which gives information about the shape and magnitude of the spread of Infectious individuals, since the presence of Infectious individuals will reduce the Susceptible population.

At first glance, it seems that altering the diffusion has the largest effect, with the contact rate β only causing a significant effect when taking the value 0.05. This perception, however, is an artifact of the visualization of the data. In each image, the colors are scaled from the minimum value to the maximum value of each image. In Figure 4.4a, that range has a magnitude of only 1.5, compared to the total population of 100. In Figure 4.4b, however, the range has expanded to reach from 90 to 100. In Figure 4.5b, the force of infection is so high that the entire Susceptible population is eliminated by the disease. From these

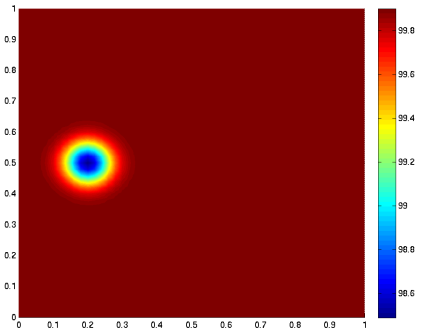

(a) $\beta = 0.001$, $\nu = 0.00005$

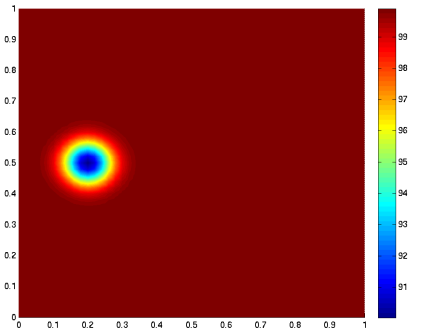

(b) $\beta = 0.005$, $\nu = 0.00005$

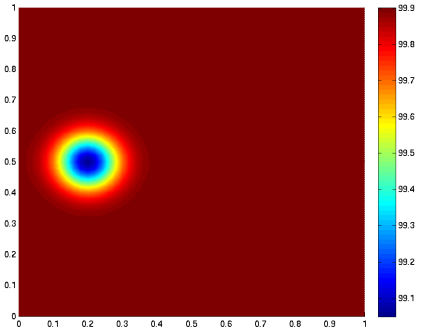

(c) $\beta = 0.001$, $\nu = 0.0001$

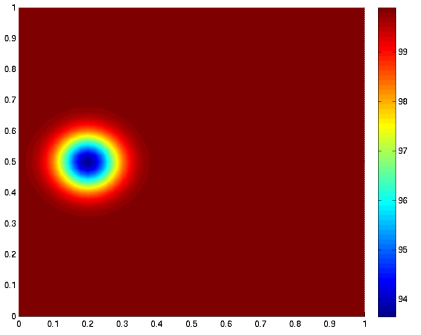

(d) $\beta = 0.005$, $\nu = 0.0001$

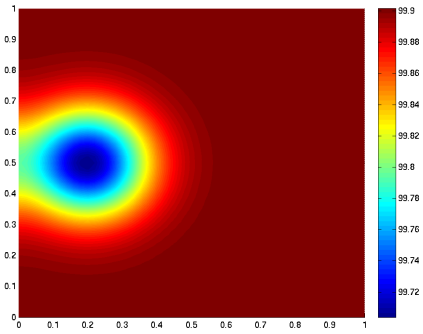

(e) $\beta = 0.001$, $\nu = 0.0005$

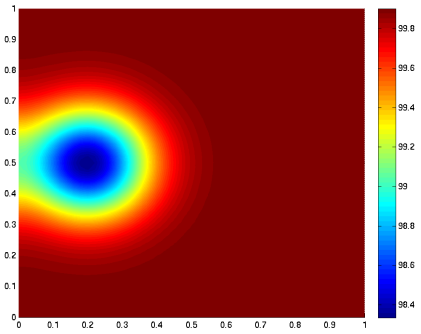

(f) $\beta = 0.005$, $\nu = 0.0005$

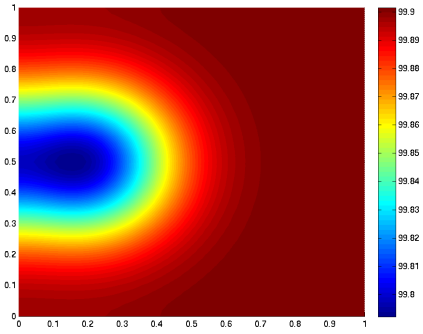

(g) $\beta = 0.001$, $\nu = 0.001$

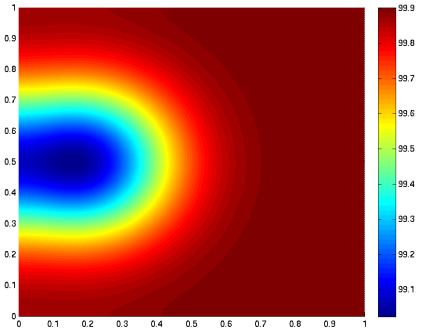

(h) $\beta = 0.005$, $\nu = 0.001$

Figure 4.4: Results from sensitivity analysis of β and ν

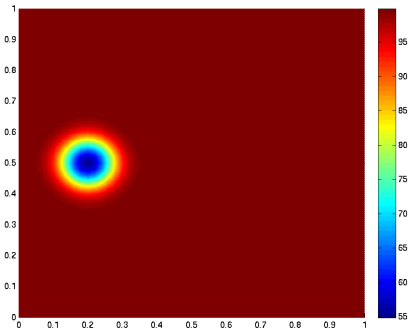

(a) $\beta = 0.01$, $\nu = 0.00005$

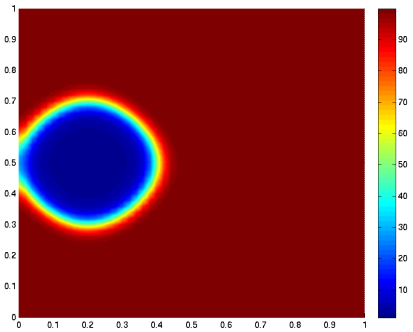

(b) $\beta = 0.05$, $\nu = 0.00005$

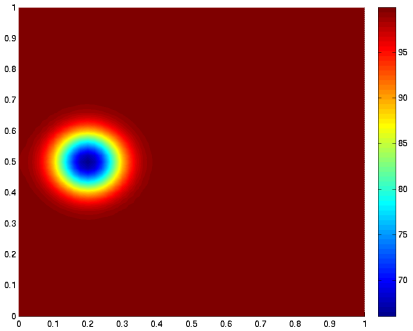

(c) $\beta = 0.01$, $\nu = 0.0001$

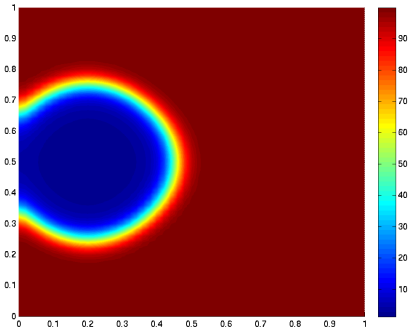

(d) $\beta = 0.05$, $\nu = 0.0001$

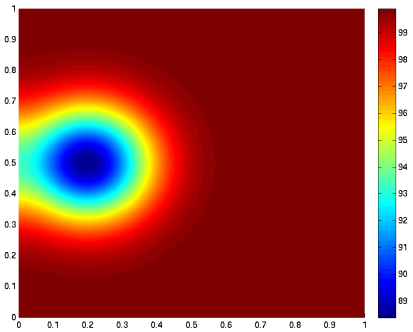

(e) $\beta = 0.01$, $\nu = 0.0005$

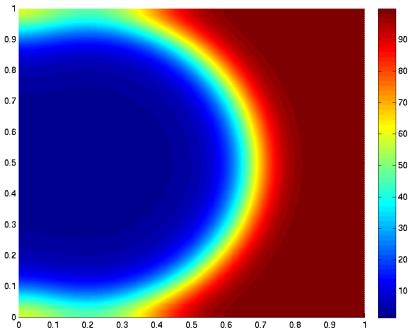

(f) $\beta = 0.05$, $\nu = 0.0005$

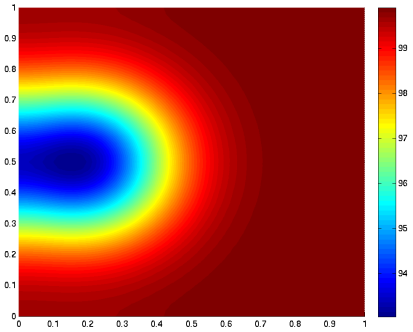

(g) $\beta = 0.01$, $\nu = 0.001$

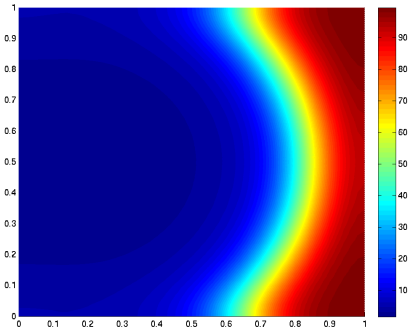

(h) $\beta = 0.05$, $\nu = 0.001$

Figure 4.5: Results from sensitivity analysis of β and ν

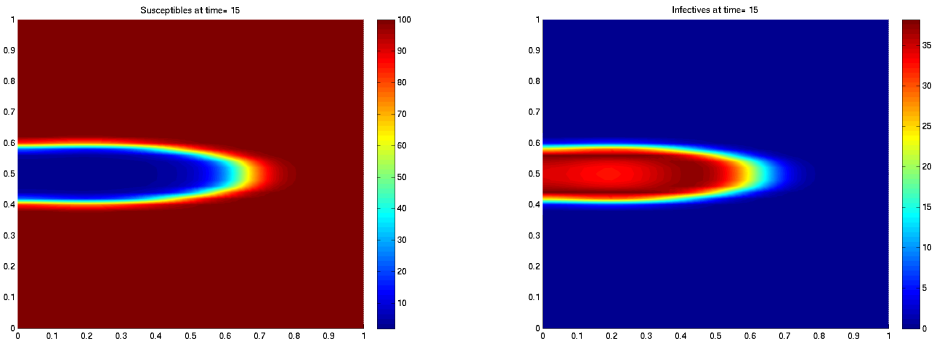

(a) Suceptible at t=15 (b) Infectious at t=15

Figure 4.6: Spread of an artificial disease over the unit square with anisotropic conditions favoring horizontal movement

simulations, it becomes apparent that while the diffusion coefficient ν controls the spatial spread of disease, the magnitude of the contact rate β has a greater impact on the disease dynamics. Even in cases of higher diffusion (Figures 4.4g and 4.4h), a low value of β means that there is almost no disease spread. In other words, the value of ν greatly affects the possibility of a single case of a disease appearing in any spatial location, but the value of β determines whether an epidemic, or at least a significant number of cases, can occur.

Lastly, we present several examples demonstrating anisotropic and non-homogeneous diffusion. The simulation performed in Figure 4.6 shows the effects of introducing anisotropy into (3.2). Here diffusion in the y-direction was reduced by a factor of 0.01, causing the disease to propagate in the x-direction. The other epidemiological parameters were identical to Figure 4.2 and $\nu_x = 0.005$.

An example of the river-border anisotropy governed by equation (3.1) can be seen in Figure 4.7a, where a "river" stretching from $(0.4, 0)$ to $(0.4, 1)$ across the domain reduces diffusion in the positive x-direction across the square. In Figure 4.7b, we can see the effect of having a region of low isotropic diffusion in the middle of the domain. Within the circle of radius 0.2 centered at (0.5,0.5), the diffusion coefficient has been lowered by a factor of

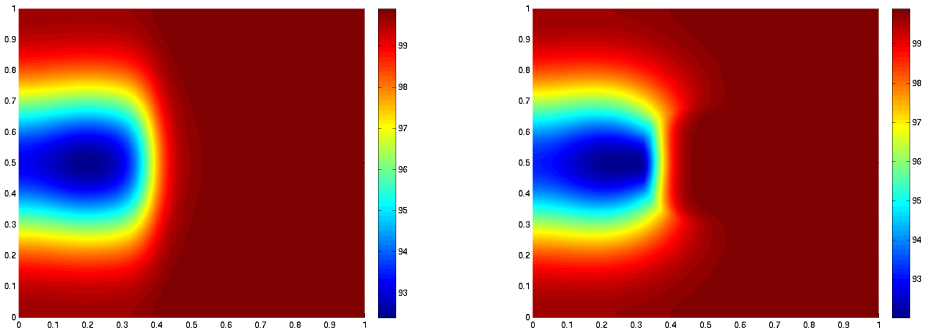

(a) Simulation with river barrier (b) Simulation with a mountainous region

Figure 4.7: Simulations of epidemics on the unit square with different factors causing anisotropic diffusion

10. This simulates a swamp, mountainous region, or other geographic area that reduces movement in all directions.

Chapter 5

Case Study: Rabies in New York

We now apply the diffusion SEIR model (3.2) to a case study on the spread of rabies in New York state. Since the 1970's when the disease was translocated from an epidemic in the Florida area, rabies has been spreading in raccoons across the mid-Atlantic region, reaching to the north and east from the Virginia-West Virginia border [31, 4, 30]. This wave of disease has resulted in over 50,000 cases of rabid raccoons throughout the region [4]. The epidemic sweeping these states is of interest in part because of its contrast with previous rabies outbreaks elsewhere. In the southeastern U.S., rabies had spread relatively slowly and there was not a high degree of cases (0.003 cases/mi^2 in 1996), while cases were significantly more prevalent in this mid-Atlantic epidemic (0.012 cases/mi^2 in 1996) [4]. Some explanations for this difference cite the higher population density of humans and more favorable habitats for raccoons in the mid-Atlantic region [4].

This wave of rabies entered the state of New York in 1990, with the first reported case occurring in May of that year. The New York State Department of Health kept records of the confirmed cases of rabies in raccoons. These data are presented in Figure 5.1. The epidemic front starts along the southern border and clearly moves to the north and east, though there seems to be a separate outbreak of cases in the northeastern portion of the

state.

While providing clear evidence of and a general shape for an epidemic front, this data is by no means complete. The data in Figure 5.1 are only the confirmed cases of rabies, and cannot be presumed to capture all of the true number of cases [25]. The number of reported cases (and thus confirmed cases) is also dependent upon the distribution of humans in the area, since a rabid raccoon in a population with high human density is more likely to be found, reported, and confirmed than one in a rural, sparsely populated region. The data and epidemic presented here are currently being analyzed using a coupled metapopulation model with a discrete approach to movement. In this case study this epidemic is analyzed using the continuous movement model (3.2).

5.1 Numerical Problem

To simulate a solution to the diffusion model (3.2) for this case study, we follow the steps presented in Chapter 4. First, a mesh of the state of New York is created. Next, we establish appropriate values for the epidemiological and diffusion parameters and select locations for the source terms. We then perform the assembly and time-advancement stages in MATLAB and present a visual representation of the results.

To generate the domain mesh for the simulations, a satellite image of New York State was obtained from http://geology.com/satellite/new-york-satellite-image.shtml (see Figure 5.2). The pixel locations at locations along the state boundary and desired geographic features (discussed below) were then selected by hand and extracted from this image using ImageJ[1]. An outline of the desired geometry was then generated by interpolating these boundary points with linear functions in NetGen. NetGen was then used to generate a triangular mesh of the state. Two meshes were created, one with 7072 nodes and 13640 elements, and

[1]http://rsbweb.nih.gov/ij/

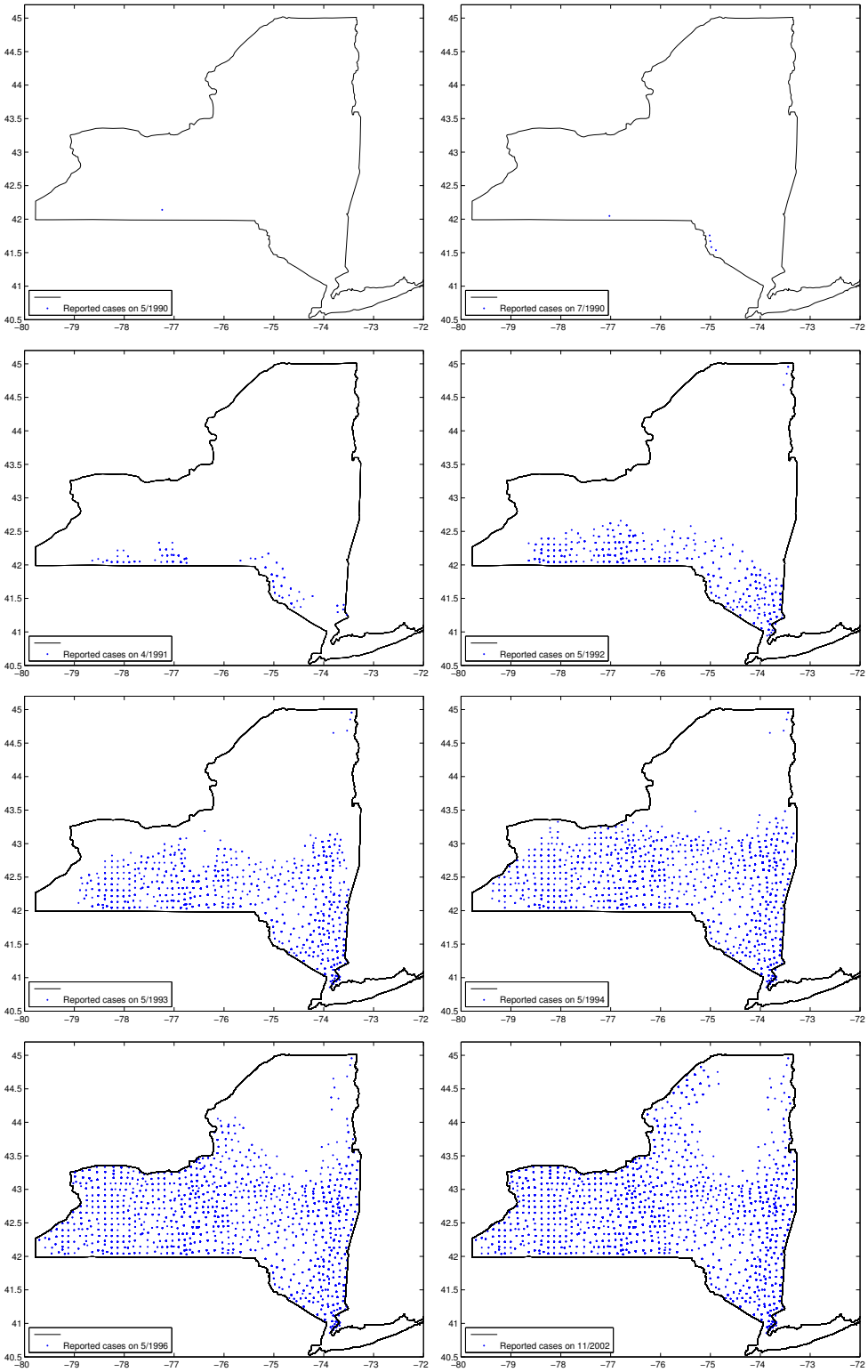

Figure 5.1: Cumulative confirmed cases of rabies in NY raccoons

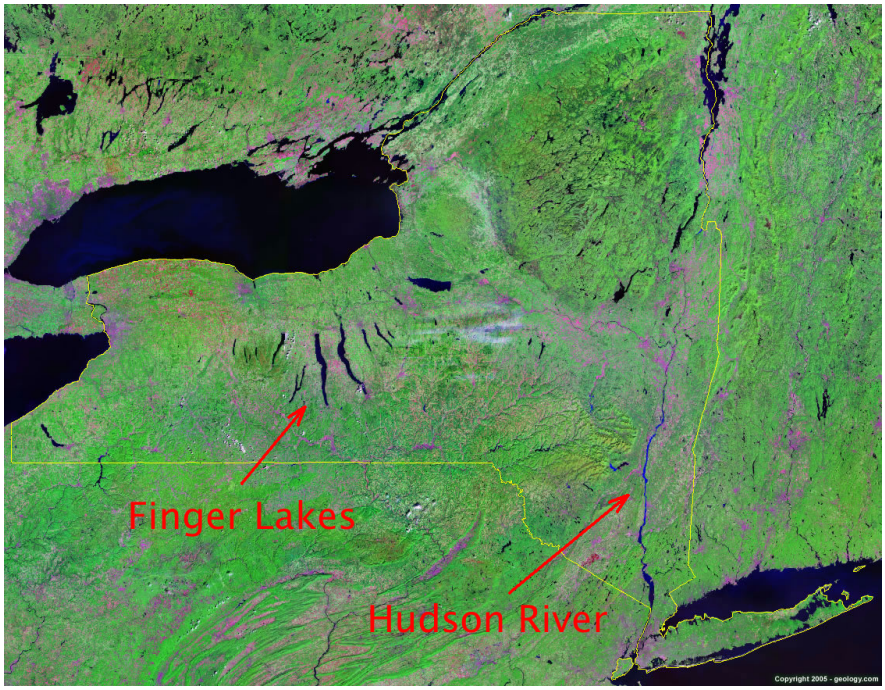

Figure 5.2: A satellite image of New York, with the Hudson River and Finger Lakes pointed out. The yellow line forms the state border.

a finer mesh with 12968 nodes and 24928 elements (see Figure 5.3). Once created, the mesh was then scaled to values of latitude and longitude, in which all coordinates will be given.

The population density of raccoons is known to vary from 5 to 17 individuals per kilometer and to be higher in areas of high human population. This gives a total raccoon population for the state of approximately 1,320,000. This population was divided equally among all of the 12968 nodes in our domain, giving an initial population of 102 at each node. Studies have shown that the average latency period of infection is approximately 50 days, that infectious individuals survive 15 days on average, and that each female raccoon produces approximately 2.67 offspring per year. For the simulations, these values were scaled so that each unit of time represented an average month of thirty days. Thus, $\sigma = 0.6$, $\phi = 2$, and $\alpha = 0.1113$.

Though the model is designed for the inclusion of vaccination, no vaccination term was included in these simulations. That is, for the simulations in New York, $\gamma = 0$.

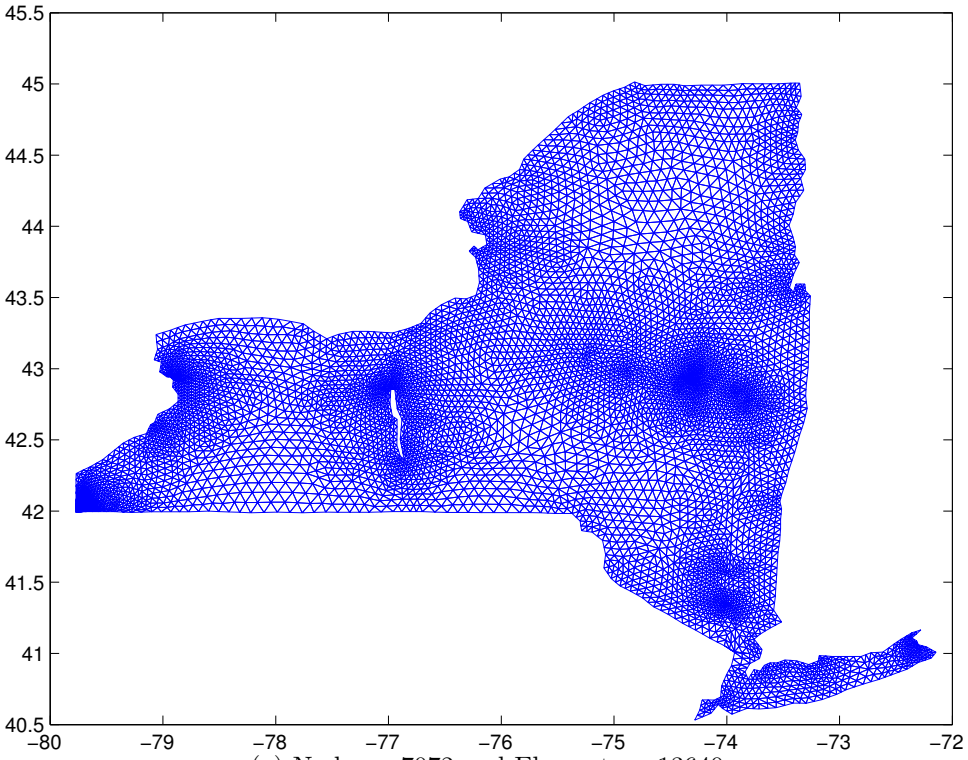

(a) Nodes = 7072 and Elements = 13640

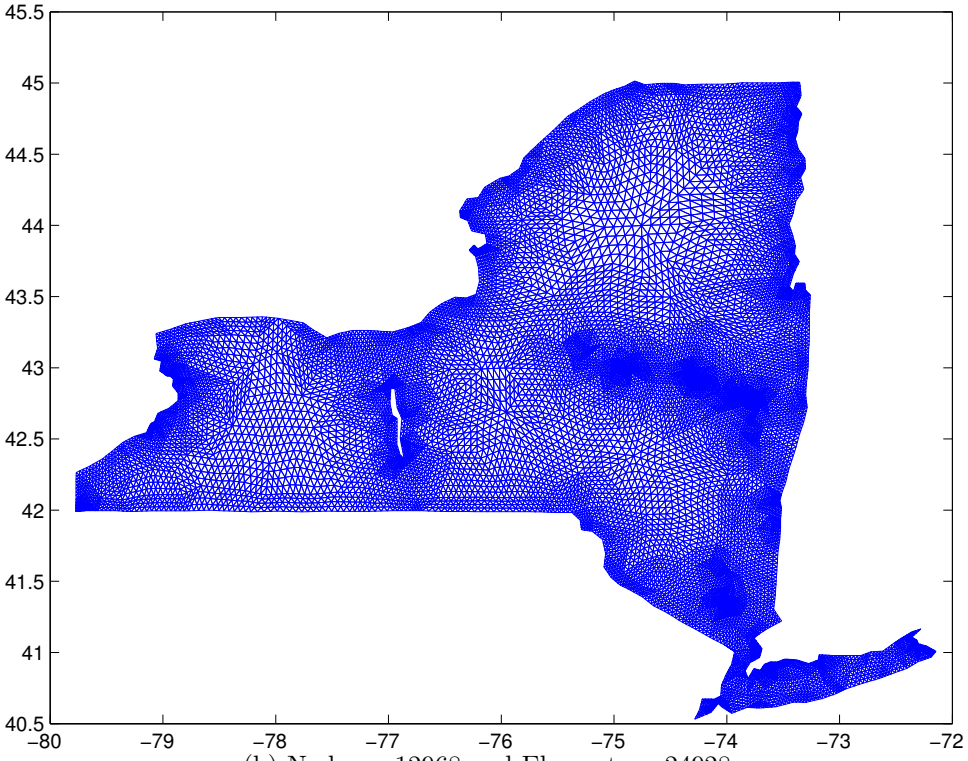

(b) Nodes = 12968 and Elements = 24928

Figure 5.3: The triangular meshes of New York

To reflect the spatial heterogeneity of the geography in New York, several spatial dependencies for the diffusion coefficient were included. In recognition of the barrier that rivers provide, we included an anisotropic layer along the Hudson river. Diffusion parallel to the river was unaltered, but diffusion across the river was drastically reduced to account for the barrier that such a body of water provides to raccoons. This was done by finding the distance from each node to the river, $\hat{x}$, and evaluating $\nu_\epsilon(\hat{x})$, where ν_ϵ is defined by (3.1). For these simulations, $\epsilon = 0.2$. This formulation allows for the diffusion tensor to be calculated perpendicular to the river as the Hudson curves and turns throughout the domain. As in any model, there must be a balance between the complexity of making the model more realistic and the simplicity that makes the model mathematically, computationally, and usefully tractable. As such, no diffusion border was created for the other rivers in the state. An examination of the data in Figure 5.1 shows that there does not seem to be any significant geographic barriers to the disease front, except for the Hudson river in the east.

Nonetheless, we wished to include additional geographic features to examine their effect on the dynamics. The Finger lakes in west-central New York are prodigious bodies of water within the state, and one of these lakes was included. In contrast to the Hudson river, across which movement was drastically reduced, movement across this lake was entirely eliminated, creating a closed internal boundary.

The population of raccoons in the mountainous region in upstate New York is less dense than elsewhere in the state, but the region is also presumed to facilitate a slower rate of movement. Therefore we introduced reduced isotropic diffusion for a circular region with radius 0.5 and center $(-74.5, 44)$. Here the diffusion was reduced by a factor of 4. This is in keeping with Figure 5.1, which shows that the front of confirmed cases appears to slow down upon approaching this region.

To best reflect the real-world data, the source terms for the epidemic were placed at the

four locations highlighted in Figure 5.4. These locations correspond to the first confirmed case of rabies in four areas of the state. Each source term was added at the time step equivalent to the first confirmed case in that region (see Figure 5.1). The western source term, centered at $(-77.29, 42.14)$, is at the location of the first confirmed case and so was introduced at $t = 0$. Also at $t = 0$, the south-central source was introduced, centered at $(-75.00, 41.67)$. Though the first case in that region (July 1990) was actually two months after the first case in the western region, this source was introduced at the beginning ($t = 0$) for simplicity. Both of these first two source terms had a circular radius of 0.2. The next source term was the south-eastern source, centered at $(-73.61, 41.33)$ with radius 0.1 and introduced at $t = 11$. This source was important because it is east of the Hudson river, allowing for the dynamics of the river anisotropy to be demonstrated. The final source term was introduced much later at $t = 25$ and is centered at $(-73.53, 44.69)$ with a radius 0.05 in the northeastern corner of the state. The cases that appeared in this area of the state were possibly introduced from the northeast, while the other cases are presumed to be a part of the wave spreading northeast from the Virginia-West Virginia border. Rather than have single point sources, these source terms introduced a certain number of infected and exposed individuals into a small circular region to allow for the disease dynamics to propagate. A source at a single node would not have a profound effect because of diffusion from the surrounding nodes.

These starting source terms do introduce some degree of bias in the model, since in reality the disease would probably have been introduced by infectious individuals migrating into New York from the states to the south and west. However, they present a means for introducing infection into the region and then allowing for the epidemic to propagate.

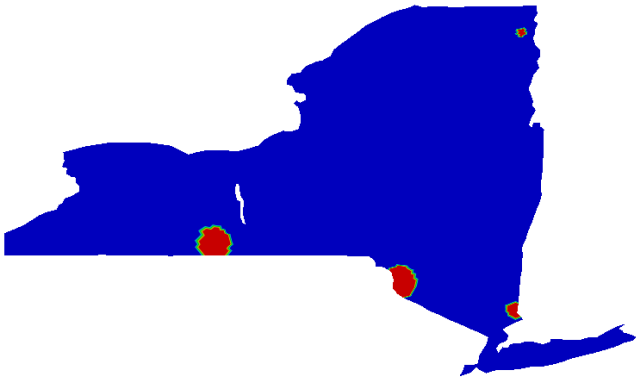

Figure 5.4: Location of source terms for simulations of (3.2) in New York. Each source region was added a different time step.

5.2 Results

In order to confirm the effectiveness of the anisotropic diffusion coefficients, a preliminary simulation was performed on the coarser mesh. The values for epidemiological parameters discussed above were used and the default diffusion coefficient was set at $\nu = 0.01$. This value of ν is arbitrary, but was selected so that the epidemic front would spread throughout the state at a speed roughly equivalent to the spread of confirmed cases in Figure 5.1. For these simulations, $S^0 = 98$ and $E^0 = I^0 = 0$ across the entire domain except for the source region of radius 0.2 with center $(-75, 42.5)$ where the initial values were $S^0 = 78$, $E^0 = 15$, and $I^0 = 5$.

The images in Figure 5.5 show the population of Susceptibles for several times throughout this epidemic simulation. As the epidemic progresses, the infection of susceptible individuals causes the Susceptible population to drop, following the same spatial pattern as the expanding disease front. In Figure 5.5a, the circular pattern characteristic of isotropic diffusion become apparent, even at $t = 1$ (which amount to 10 time-steps, since $\Delta t = 0.1$). At $t = 10$ in Figure 5.5b, one can see the effect of the Hudson river boundary slowing the spread to

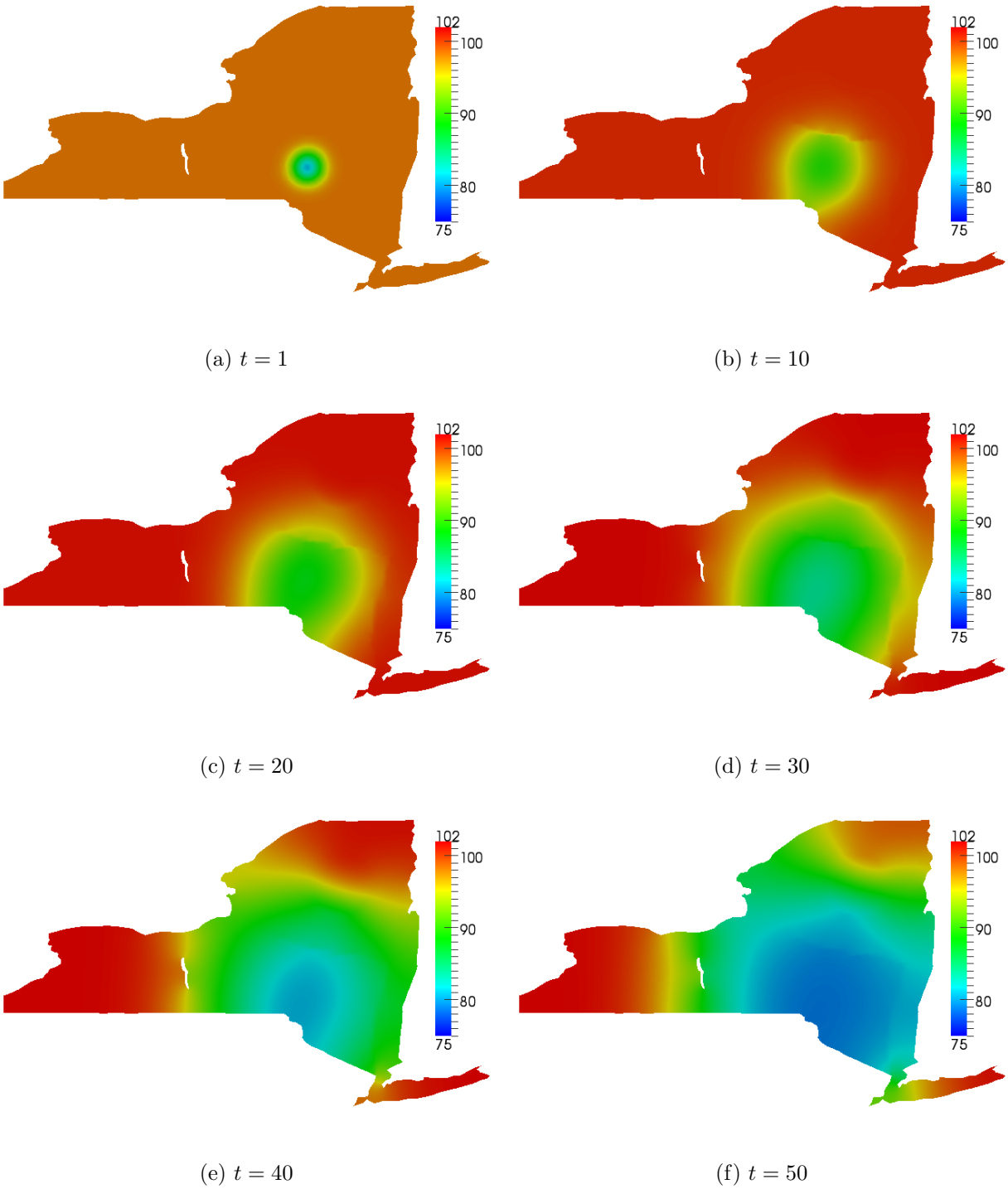

(a) $t = 1$

(b) $t = 10$

(c) $t = 20$

(d) $t = 30$

(e) $t = 40$

(f) $t = 50$

Figure 5.5: The Susceptible population in an artificial epidemic simulation on New York, demonstrating the effects of geographically-based diffusion.

the north. In Figures 5.5c, the river is still reducing the rate of diffusion to the north, and we begin to see the effect of the river to the east as well. One hundred time-steps later at $t = 30$ in 5.5d, we can see the effect of the river limiting diffusion to the east and the effects of the reduced diffusion in the mountain region in the north. Even though the western front of the epidemic is advancing perpendicular to the Finger Lake, we note that in Figures 5.5e and 5.5f the lake seems to have little effect on the spread, though there is a slight shielding effect visible in Figure 5.5e.

After the preliminary simulation confirmed the effective presence of the anisotropy, the primary simulation for the case study was performed. Here again, the epidemiological parameters took the values given in the previous Section. This simulation was performed on the finer mesh of New York, and here again $\nu = 0.01$. The source terms, both initial and delayed, were included as described in the previous section.

Figures 5.6-5.8 show the spread of the Susceptible, Exposed, and Infectious classes for several snapshots in time.

The most striking feature of these results is the disease front that moves out from the source regions, which appears to reach out in a similar manner to the reported data. This indicates that the diffusion model can at least qualitatively reproduce the effects of a reported epidemic. As expected from the general isotropic diffusion throughout most of the state, this front takes on a circular shape. The reported cases in Figure 5.1 spread out in a less discernible shape, since they are part of a larger epidemic front that began outside of New York. This difference seems most noticeable in the western portion of the state, along the southern border with Pennsylvania. In the simulation in Figure 5.8, the epidemic moves directly westward, while the reported cases seem to be coming up from the south. This highlights one weakness of the model, in that by isolating the state of New York, we cannot fully capture the present dynamics, especially at the onset of the epidemic.

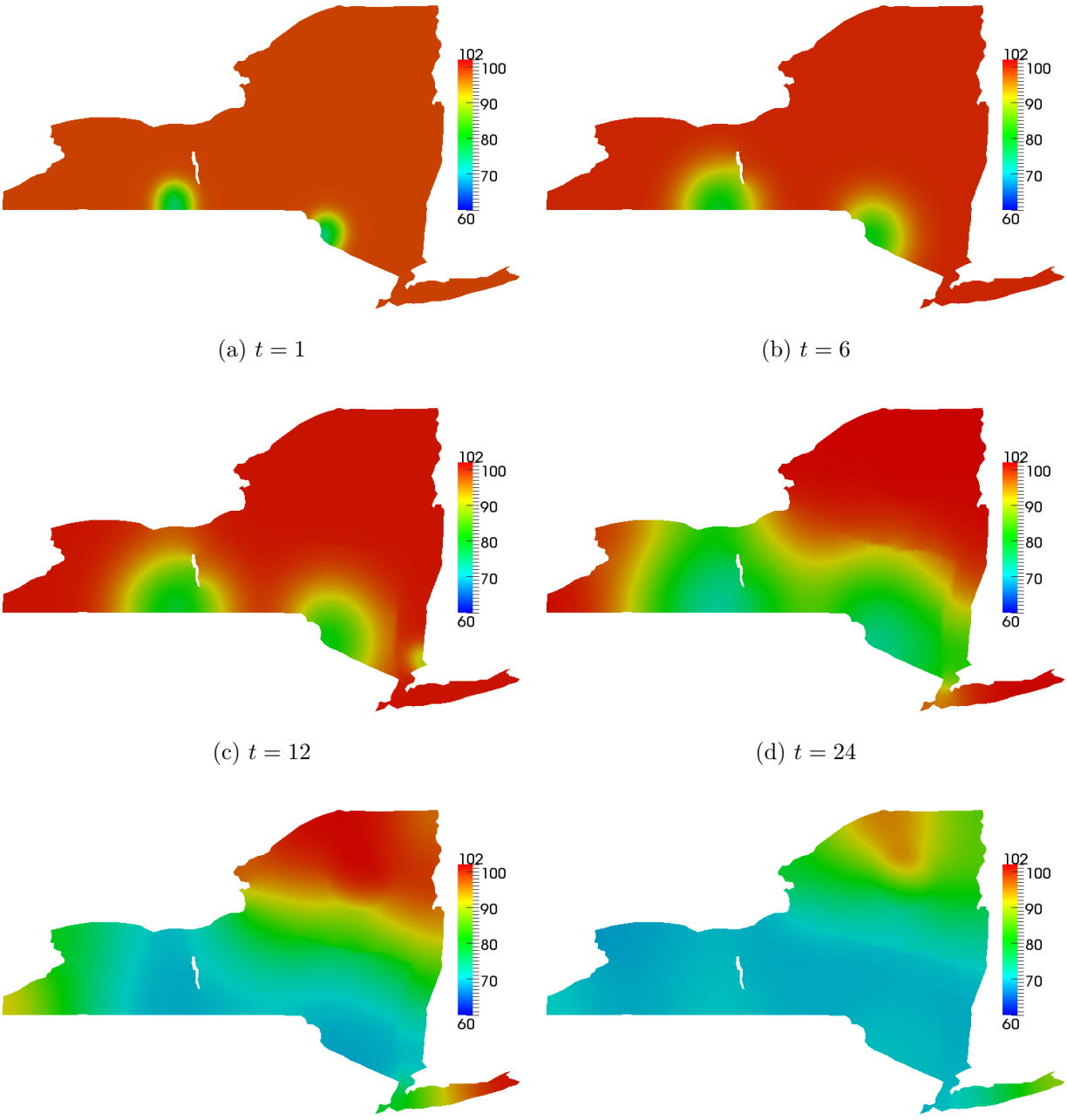

(a) $t = 1$ (b) $t = 6$

(c) $t = 12$ (d) $t = 24$

(e) $t = 36$ (f) $t = 48$

Figure 5.6: The population of Susceptible individuals for t measured in months

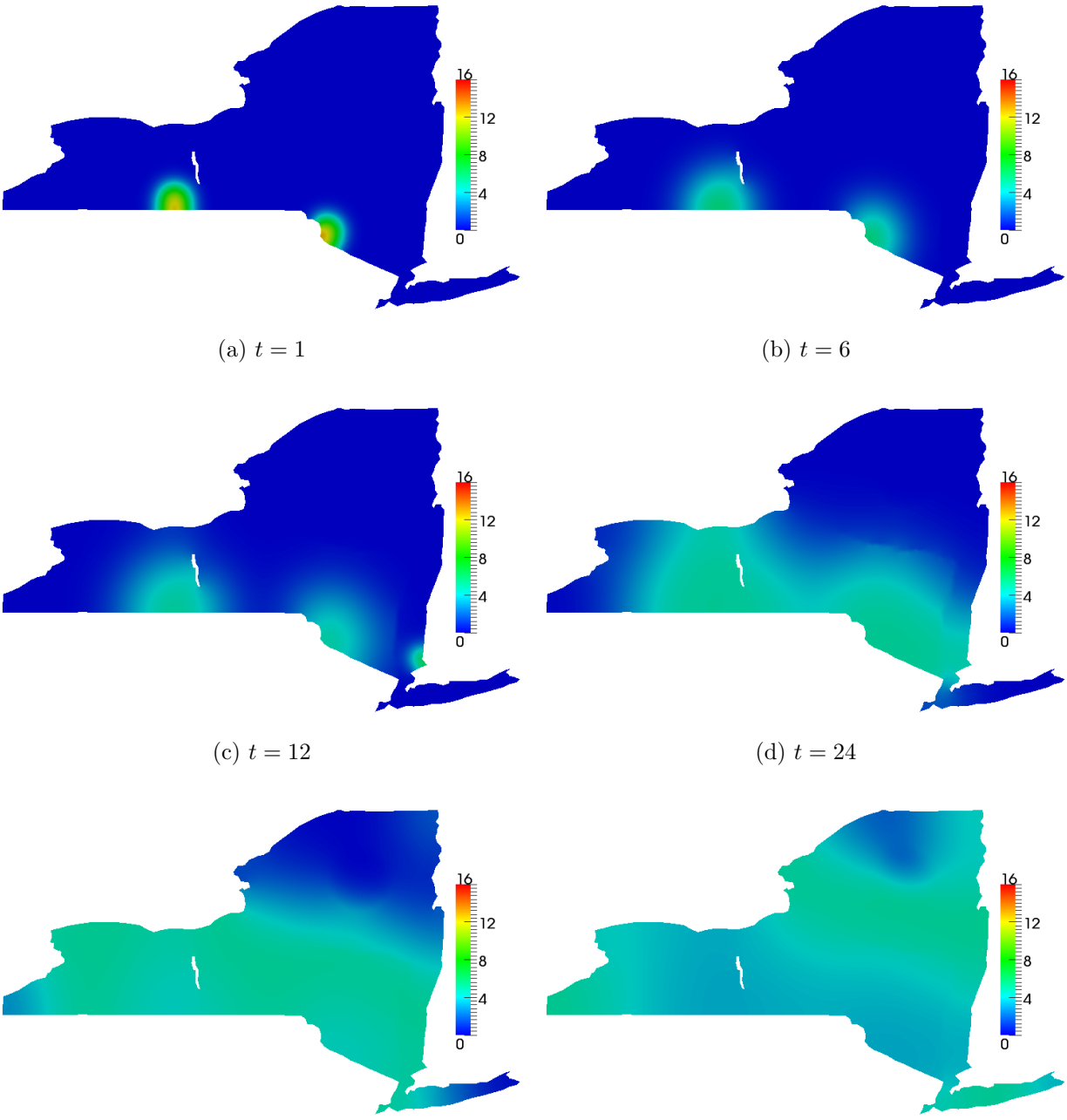

(a) $t = 1$ (b) $t = 6$

(c) $t = 12$ (d) $t = 24$

(e) $t = 36$ (f) $t = 48$

Figure 5.7: The population of Exposed individuals for t measured in months

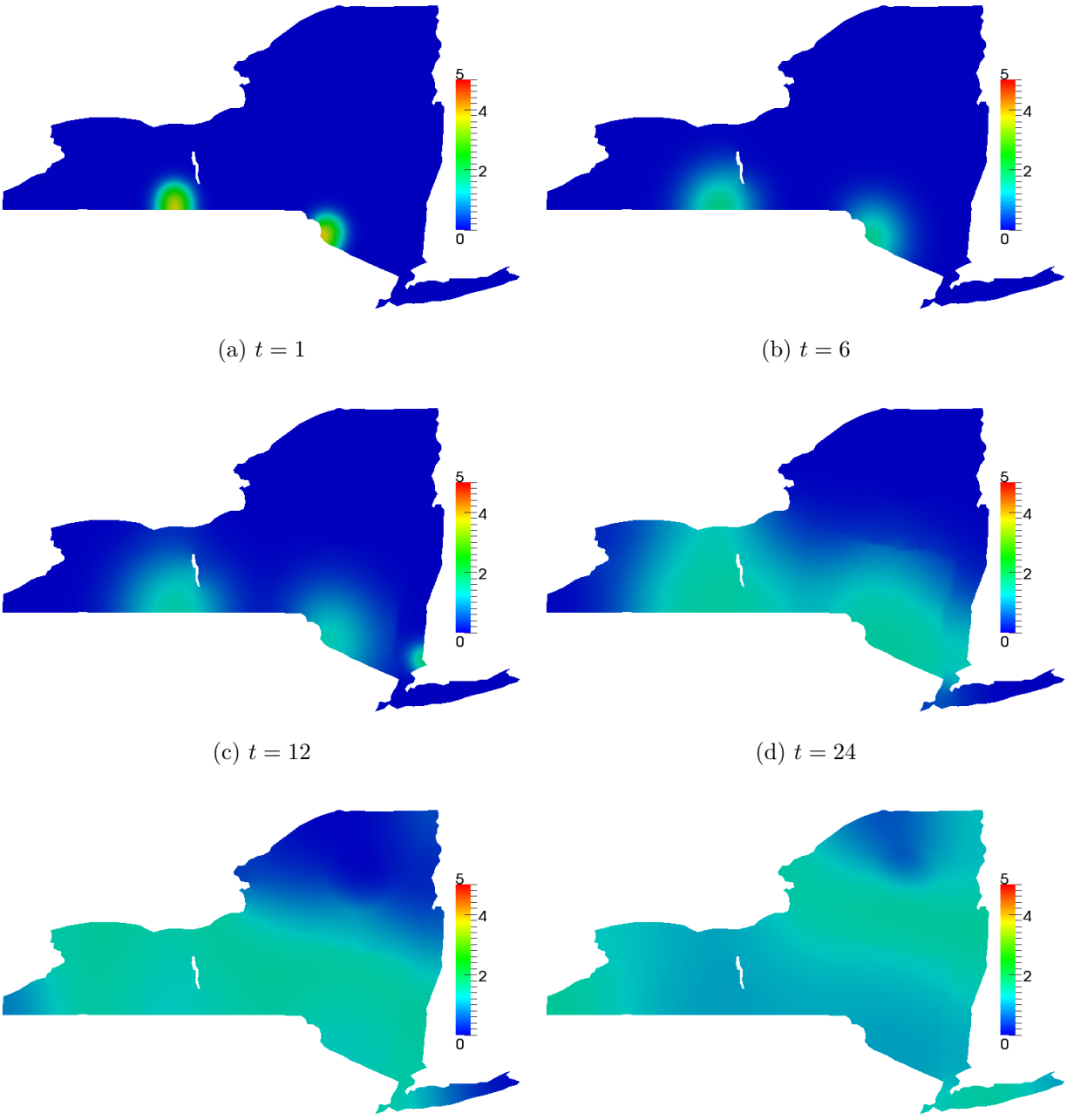

(a) $t = 1$ (b) $t = 6$

(c) $t = 12$ (d) $t = 24$

(e) $t = 36$ (f) $t = 48$

Figure 5.8: The population of Infectious individuals for t measured in months

The Finger Lake is orientated along a north-south axis, while the rabies is spreading from the south to the north. Because of this, we did not expect the inclusion of the lakes in our model to have a significant effect on the advancement of the disease front. The images in Figure 5.6 show that the lakes did not have a significant effect on the spread the disease. This lack of effect demonstrates how even relatively large geographical features can have a minor effect on disease spread, and the decision to exclude or include features in a model should be made with care. While the inclusion of a feature with little effect should not harm the accuracy of a model, the additional technical complexities and computational requirements it imposes can reduce the efficacy of the model.

In addition to the diffusion generating the expected behavior in the model, the quantitative results of the simulation are epidemiologically reasonable and coherent with expected results. Figure 5.9 shows the populations of each compartment at a single node inside the source region. By looking at this local population, we can see the effects of the epidemic on the relative populations of each category. In the first ten months, the populations of Exposed and Infectious individuals drop, while the population of Susceptibles increases in number. This can be expected since the initial values for each category are partially arbitrary and do not represent a stable equilibrium. The reason this shift is towards less Infectious and more Susceptible individuals (and not more Infectious and less Susceptibles) is in part due to the disease-induced mortality in the Infectious class. The high rate of death for Infectious individuals reduces that population initially, before sufficient individuals are infected and the epidemic propagates.

After the initial peak in the Susceptible population, the epidemic begins to take hold and the Susceptible population drops, just as the the Exposed and Infectious populations rise. When viewed on the same graph (Figure 5.9d), the rise in Exposed and Infectious individuals seems inconsequential to the total population or even the noticeable drop in the

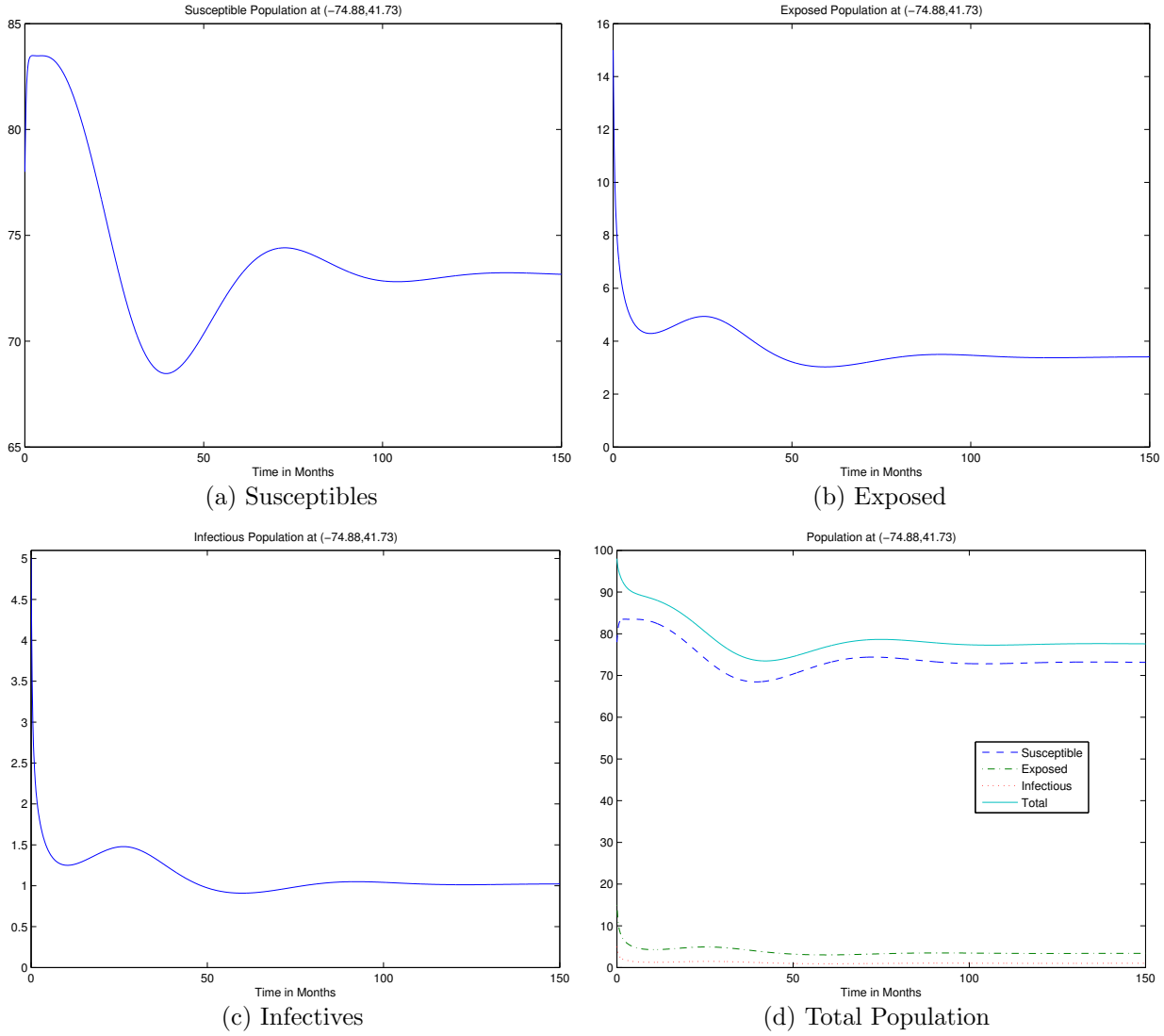

(a) Susceptibles (b) Exposed

(c) Infectives (d) Total Population

Figure 5.9: The population at the node at (-74.88,41.73)

Susceptible population. However the increase is sufficient to create the epidemic front present in 5.6. About 100 months after the initial cases, the populations of all three categories have a reached a stable level. In this simulation, $R_0 \approx 1.27$, and so we expect to see the Susceptible population drop to approximately $N/R_0 = 77.16$ according to our analysis in Sections 3.3 and 2.3.1. The equilibrium population of approximately 77.54 in Figure 5.9d supports this.

Chapter 6

Conclusions

The results of this case study show that an epidemiological model with a diffusion component can model disease dynamics with a large degree of accuracy. The diffusion model seems especially well suited to modeling movement in situations in which there is significant geographical heterogeneity. The ease with which the diffusion coefficients may be adjusted makes including such factors feasible. The inclusion of spatially-dependent diffusion values, however, requires judicious selection of appropriate geographic features to include.

Despite the power of this model to simulate the spread of disease, this continuous approach does not eliminate the need for the discrete approach that is also in use. When including data that is already organized according to geopolitical units, as is usually the case for public health centers, the discrete model can accommodate this data more readily than the continuous model. The discrete metapopulation model can also be appropriate for situations where individuals are clustered into regions and not uniformly spread throughout a region. A prime example of this would be the distribution of humans in cities and towns.

These differences suggest that the continuous-movement model would be well-suited to a predictive role in epidemiology, while the discrete model would work well in fitting models to previously existing data. In fitting a discrete model to the data, the necessary parameter

tuning could shed light on regions where geographical features may have a significant effect, and thus should be considered for inclusion in the predictive continuous model. However, one should use care when comparing parameters between models. Models developed for different purposes and with different assumptions should not be used interchangeably.

In both models, parameter estimation plays a key role, since even the slightest alteration can dramatically affect disease dynamics. The parameters presented here were all deterministic, but in advanced models they are often included as stochastic variables. Each parameter can vary depending upon location, disease, time, and individual. The process of estimating consistent and unbiased values for these parameters remains an area of active research.

Bibliography

[1] R.M. Anderson. Discussion: The Kermack-McKendrick epidemic threshold theorem. *Bulletin of Mathematical Biology*, 53(3-32), 1991.

[2] V. Capasso. *Mathematical Structures of Epidemic Systems*. Springer-Verlag, 1991.

[3] T. Caraco, S. Glavanakov, G. Chen, J.E. Flaherty, T.K. Ohsumi, and B.K. Szymanski. Stage-structured infection transmission and a spatial epidemic: A model for lyme disease. *American Naturalist*, 160:348–359, 2002.

[4] J.E. Childs, A.T. Curns, M.E. Dey, L.A. Real, C.E. Rupprecht, and J.W. Krebs. Rabies epizootics among raccoons vary along a north-south gradient in the eastern United States. *Vector Borne and Zoonotic Diseases*, 1(4):253–267, 2001.

[5] Y.V. Egorov and M.A. Shubin. *Linear Partial Differential Equations: Foundations of the Classical Theory*. Springer-Verlag, 1991.

[6] W.E. Fitzgibbon, M.E. Parrott, and G.F. Webb. Diffusion epidemic models with incubation and crisscross dynamics. *Mathematical Biosciences*, 128:131–155, 1995.

[7] D. Greenhalgh. Some threshold and stability results for epidemic models with a density-dependent death rate. *Theoretical Population Biology*, 42:130–151, 1992.

[8] W.H. Hamer. Epidemic diseases in England–the evidence of variability and of persistency of type. *Lancet*, 1(733-739), 1906.

[9] J.M. Heffernan, R.J. Smith, and L.M. Wahl. Perspectives on the basic reproductive ratio. *Journal of the Royal Society Interface*, 2:281–293, 2005.

[10] E.E. Holmes, M.A. Lewis, J.E. Banks, and R.R. Veit. Partial differential equations in ecology: Spatial interactions and population dynamics. *Ecology*, 75:17–29, 1994.

[11] W. Hundsdorfer and J. Verwer. *Numerical Solution of Time-Dependent Advection-Diffusion-Reaction Equations*. Springer, 2003.

[12] F. John. *Partial Differential Equations*. Applied Mathematical Sciences. Springer-Verlag, New York, fourth edition, 1982.

[13] M.J. Keeling and P. Rohani. *Modeling Infectious Disease in Humans and Animals*. Princeton U Press, 2008.

[14] W.O. Kermack and A.G. McKendrick. A contribution to the mathematical theory of epidemics. *Proc. Roy. Soc. Lond.*, 115(700-721), 1927.

[15] P.E. Lewis and J.P. Ward. *The finite element method: prinicples and applications*. Addison-Wesley, 1991.

[16] M.Y. Li and J.S. Muldowney. Global stability for the seir model in epidemiology. *Mathematical Biosciences*, 125:155–164, 1995.

[17] A.L. Lloyd and V.A.A. Jansen. Spatiotemporal dynamics of epidemics: synchrony in metapopulation models. *Mathematical Biosciences*, 188:1–16, 2004.

[18] R.M.M. Mattheij, S.W. Rienstra, and J.H.M. ten Thije Boonkkamp. *Partial Differential Equations: Modeling, Analysis, Computation*. SIAM, 2005.

[19] R.M. Anderson R.M. May. *Infectious Diseases of Humans: Dynamics and Contrl*. Oxford Science Publications, 1991.

[20] G.D. Murray and A.D. Cliff. A stochastic model for measles epidemics in a multi-region setting. *Transactions of the Institute of British Geographers*, 2:158–174, 1977.

[21] J.D. Murray, E.A. Stanley, and D.L. Brown. On the spatial spread of rabies amoung foxes. *Proc. Roy. Soc. Lond.*, 229:111–150, 1986.

[22] J.V. Noble. Geographic and temporal development of plagues. *Nature*, 250:726–728, 1974.

[23] A. Quarteroni, R. Sacco, and F. Saleri. *Numerical Mathematics*. Springer, 2000.

[24] A. Quarteroni and A. Valli. *Numerical Approximation of Partial Differential Equations*. Springer, 19914.

[25] L.A. Real and J.E. Childs. Spatial-temporal dynamics of rabies in ecological communities. In S.K. Collinge and A.C. Ray, editors, *Disease Ecology: Community structure and pathogen dynamics*, chapter 12, pages 168–185. Oxford Univ. Press, 2006.

[26] S. Ruan. Spatial-temporal dynamics in nonlocal epidemiological models. In *Mathematics for Life Science and Medicine*, pages 97–122. Springer, 2007.

[27] C.E. Rupprecht, J.S. Smith, M.F. Fekadu, and J.E. Childs. The ascensino of wildlife rabies: A cause for public health concern or intervention? *Emerging Infectious Diseases*, 1:107–114, 1995.

[28] S. Salsa. *Partial Differential Equations in action: From modelling to theory.* Springer, 2009.

[29] L. Sattenspiel and K. Dietz. A structured epidemic model incorporating geographic mobility among regions. *Mathematical Biosciences*, 128:71–91, 1995.

[30] D.L. Smith, B. Lucey, L.A. Waller, J.E. Childs, and L.A. Real. Predicting the spatial dynamics of rabies epidemics on heterogeneous landscapes. *PNAS*, 99(6):3668–3672, 2002.

[31] J.S. Smith, J.W. Sumner, L.F. Roumillat, G.M. Baer, and W.G. Winkler. Antigenic characteristics of isolates associated with a new epizootic of raccoon rabies in the united states. *Journal of Infectious Disease*, 149:769–774, 1984.

[32] R.T. Sterner and G.C. Smith. Modelling wildlife rabies: Transmission, economics, and conservation. *Biological Conservation*, 131:163–179, 2006.

[33] P. van den Driessche. Spatial structure: Patch models. In F. Brauer, P. van den Driessche, and J. Wu, editors, *Mathematical Epidemiology*, Lecture Notes in Mathematics, chapter 7, pages 179–189. Springer, 2008.

[34] G.F. Webb. A reaction-diffusion model for a deterministic diffusive epidemic. *Journal of Mathematical Analysis and Applications*, 84:150–161, 1981.